Extremum Seeking With Enhanced Convergence Speed for Optimization of Time-Varying Steady-State Behavior of Industrial Motion Stages

Leroy Hazeleger, Jeroen van de Wijdeven, Mark Haring, and Nathan van de Wouw, *Fellow, IEEE*

***Abstract*— Recently, an extremum-seeking control (ESC) approach has been developed for optimization of generically time-varying steady-state responses of nonlinear systems. A generic filter structure was introduced, the so-called dynamic cost function, which has been instrumental in facilitating the use of ESC in the more generic, time-varying context. However, the dynamic cost function must operate sufficiently slow compared to the time-varying nature of the system responses, thereby compromising the convergence speed of the ESC scheme. In this work, a modified ESC approach is proposed that incorporates explicit knowledge about the user-defined dynamic cost function, able to enhance the convergence speed of the ESC scheme. Moreover, we provide a stability analysis for this extended approach. The main contribution of this work is the experimental demonstration of both ESC approaches for the performance optimal tuning of a variable-gain control (VGC) strategy employed on a high-accuracy industrial motion stage setup, exhibiting generically time-varying steady-state responses. VGC is able to enhance the system performance by balancing the typical linear control tradeoff between low-frequency disturbance suppression properties and sensitivity to high-frequency disturbances in a more desirable manner. We experimentally show that, for the unknown disturbance situation at hand, the variable-gain controller can be automatically tuned using both ESC approaches to achieve the optimal system performance. In addition, enhanced convergence speed with the modified ESC approach is evidenced experimentally.**

***Index Terms*— Extremum-seeking control (ESC), industrial motion systems, performance optimization, time-varying systems.**

Manuscript received April 20, 2020; revised December 13, 2020; accepted January 18, 2021. Manuscript received in final form February 14, 2021. This work was supported in part by the CHAMeleon Research Program through the Netherlands Organisation for Scientific Research (NWO) under Project 13896. Recommended by Associate Editor G. Pin. *(Corresponding author: Leroy Hazeleger.)*

Leroy Hazeleger is with the Department of Mechanical Engineering, Eindhoven University of Technology, 5600 MB Eindhoven, The Netherlands (e-mail: l.hazeleger@tue.nl).

Jeroen van de Wijdeven is with ASML Research, 5504 DR Veldhoven, The Netherlands (e-mail: jeroen.van.de.wijdeven@asml.com).

Mark Haring is with SINTEF Digital, Mathematics, and Cybernetics, 7491 Trondheim, Norway (e-mail: mark.haring@sintef.no).

Nathan van de Wouw is with the Department of Mechanical Engineering, Eindhoven University of Technology, 5600 MB Eindhoven, The Netherlands, and also with the Department of Civil, Environmental and Geo-Engineering, University of Minnesota, Minneapolis, MN 55455 USA (e-mail: n.v.d.wouw@tue.nl).

Color versions of one or more figures in this article are available at https://doi.org/10.1109/TCST.2021.3059748.

Digital Object Identifier 10.1109/TCST.2021.3059748

I. Introduction

EXTREMUM-SEEKING control (ESC) is a data-driven and model-free method for optimizing the steady-state behavior of a stable or stabilized plant in real time, by automated adaptation of tunable plant parameters. Often in the ESC literature, the general requirement for optimizing a stable or stabilized plant is the existence of a (unknown) time-invariant parameter-to-steady-state performance map, i.e., a static input–output relationship between tunable plant parameters and the steady-state plant performance (see [2], [23], [25], [39]). In those works, the steady-state performance map characterizes the performance of the dynamical plant to-be optimized in an equilibria setting. Even in the presence of (high-frequency) noise, convergence toward a neighborhood of the optimum can be achieved, the size of which is often dependent on the noise level (see [11], [35], [37], [42]).

In cases where periodic time-varying steady-state behavior characterizes system performance, often induced by periodic disturbances acting on the system dynamics, ESC methods have been proposed in [10], [12], and [41]. To cope with a more generic problem setting, recently, an ESC method has been proposed to optimize generically time-varying steady-state behavior of a class of nonlinear systems (see [13], [14]). Considering generically time-varying steady-state plant behavior is essential, especially in practice. Namely, the steady-state performance of many industrial applications is related to generically time-varying system responses. For example, time-varying behavior emerges in reference tracking or disturbance attenuation problems, which are encountered, for example, in industrial positioning stages commonly found in pick-and-place systems, robotics, electron microscopes, and wafer scanning systems.

Other works, which have studied ESC in the presence of time-varying system behavior, are, e.g., [31]–[33]. Here, ESC is utilized directly as feedback control, able to, on the one hand, control unstable and time-varying input-affine systems and, on the other hand, optimize steady-state *equilibria* in the presence of measurement noise. The methods have been experimentally demonstrated in, e.g., [29] and [30]. We care to emphasize that, in the current work, we consider the problem of optimizing generically *time-varying* steady-state responses of stable or stabilized systems, which is a different problem

setting from the one considered in [31]–[33]. Moreover, the methods in [31]–[33] typically rely on high dither frequencies relative to the time-varying system dynamics, while the ESC method proposed in this work can employ small dither frequencies relative to the time-varying system dynamics, even in the presence of high-frequency disturbances. In addition, in the case of ESC for already stable or stabilized systems, the class of systems considered in our work is more general.

ESC for problems that involve slowly time-varying performance maps are considered in, e.g., [6], [8], [9], and [28]. Here, optimal plant performance is obtained by tracking optimal, slowly time-varying, plant parameters. We remark that this problem setting is different from the one considered in this work. We consider the problem of optimizing *static* performance maps in the spirit of [12], [20], and [41], which, however, characterize the performance in terms of generically time-varying steady-state responses (e.g., induced by time-varying disturbances). We propose an ESC method that seeks constant plant parameter settings that optimize steady-state plant performance in terms of time-varying steady-state system responses.

To facilitate the use of ESC in the more generic, time-varying context, in [14] (and preliminary results in [13]), a generic filter structure was introduced, the so-called dynamic cost function. However, to warrant sufficient time-scale separation in the ESC scheme, the dynamic cost function must operate sufficiently slow compared to the time-varying nature of the system responses, thereby compromising the convergence speed of the ESC scheme. By considering a particular linear-time-invariant (LTI) filter structure for the user-defined dynamic cost function design, in this work, a modified ESC approach is proposed that incorporates this LTI filter structure, which can enhance the convergence speed of the ESC scheme compared to the nominal ESC design in [13] and [14].

In this work, we will, in addition, experimentally demonstrate both ESC approaches by performance optimal tuning of a variable-gain control (VGC) strategy applied to an industrial motion control application. VGC can enhance the system performance by balancing the typical tradeoff between the use of low-gain and high-gain feedback control in linear motion control systems and has been the topic of many studies (see [15]–[17], [21], [36], [40], [43]). Due to the well-known waterbed effect (see [7], [34]), increasing the bandwidth of linear motion control systems by applying high-gain control to improve the ability to suppress low-frequency disturbances comes at the expense of increased sensitivity to high-frequency disturbances and noise. Instead, VGC enables a higher gain, and thus a higher bandwidth, only when necessary. However, the ability to achieve optimal performance ultimately relies on the tuning of the variable-gain controller, which can be far from trivial as system performance highly depends on the unknown disturbance situation at hand.

Automatic tuning of (nonlinear) control strategies for optimal performance has been studied in many works (see [3], [5], [18], [19], [21], [22], [24], [26]). We propose to tune VGC through ESC here as an alternative means to achieve optimal performance, which does not require knowledge on the plant model as in, e.g., [21], [22], and [24], specific (linear parameterized) controller structures as in, e.g., [5], specific experiments as in, e.g., [18] and [19], or disturbance knowledge as in [26]. In [20], ESC has been applied in the scope of periodic steady-state system behavior for the adaptive design of variable-gain controllers.

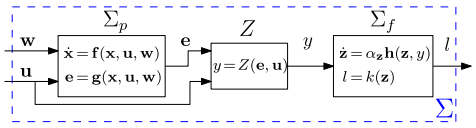

Fig. 1. Extended plant Σ, i.e., series connection of the nonlinear system Σ_p, the user-defined cost function Z, and the to-be-designed filter Σ_f.

The main contributions of this article can be summarized as follows. The first contribution is an extension of the ESC design employed in [13] and [14]. The extension involves the incorporation of explicit knowledge of LTI-structured dynamic cost function designs in the ESC design, which enables enhanced convergence speed of the ESC scheme compared to the nominal ESC design. The effectiveness is shown using a simulation example. The second contribution is a stability analysis of the closed-loop ESC scheme with the extended approach. The third contribution is the experimental demonstration of the optimization of time-varying steady-state responses of nonlinear systems using both the nominal ESC approach and the extended ESC approach presented in this work. In particular, we employ both ESC to optimally tune a VGC strategy employed on an industrial motion stage setup, which is subject to unknown and time-varying (external) disturbances. We show the effect of the design of the dynamic cost function on the convergence of the closed-loop ESC scheme. The effectiveness of the modified ESC design in terms of enhanced convergence speed with respect to the nominal ESC approach is shown experimentally as well.

This article is organized as follows. Section II presents the ESC approach for systems with time-varying steady-state responses, as well as the extended approach and its closed-loop stability analysis. Section III presents the industrial motion control application under study. Section IV presents the experimental results of both ESC strategies. Section V closes with conclusion.

II. Extremum-Seeking for Optimizing Generically Time-Varying Steady-State Behavior

In this section, first, we will briefly discuss the ESC problem formulation for generically time-varying system responses and the ESC design as studied in [13] and [14]. Second, we propose a modified ESC approach based on explicit knowledge about the dynamic cost function to enhance convergence speed compared to the initial ESC design. Third, we present a stability result of the closed-loop ESC scheme with a modified ESC approach.

A. Extremum-Seeking Control Problem Formulation

In this section, we elaborate on the elements of the so-called extended plant Σ as shown in Fig. 1, i.e., the series connection of a to-be-optimized, nonlinear system Σ_p that may exhibit

generically time-varying behavior in steady-state conditions, and a so-called dynamic cost function, consisting of a user-defined cost function Z and a user-defined filter Σ_f. This dynamic cost function has proven instrumental to achieve extremum-seeking in the time-varying steady-state setting.

1) Nonlinear System Σ_p: We consider the following generic description of a multiple-input–multiple-output nonlinear system:

$$\Sigma_p : \begin{cases} \dot{\mathbf{x}}(t) = \mathbf{f}(\mathbf{x}(t), \mathbf{u}(t), \mathbf{w}(t)) \\ \mathbf{e}(t) = \mathbf{g}(\mathbf{x}(t), \mathbf{u}(t), \mathbf{w}(t)) \end{cases} \tag{1}$$

where $\mathbf{x} \in \mathbb{R}^{n_\mathbf{x}}$ denotes the state of the system, $\mathbf{u} \in \mathbb{R}^{n_\mathbf{u}}$ denotes the input of the system, $\mathbf{e} \in \mathbb{R}^{n_\mathbf{e}}$ denotes the output of the system, $\mathbf{w} \in \mathbb{R}^{n_\mathbf{w}}$ are disturbances, and $t \in \mathbb{R}$ is time. In the context of ESC, Σ_p represents the system to be optimized, where the input $\mathbf{u}$ can be regarded as a vector of tunable system parameters, the output $\mathbf{e}$ can be regarded as a vector of measured performance variables, and $\mathbf{w}$ are piecewise continuous (time-varying and typically unknown) disturbances, defined and bounded on $t \in \mathbb{R}$. We denote this class of disturbances by $\overline{\mathbb{PC}}_\mathbf{w}$ and define the following set of disturbances $\mathcal{W} = \{\mathbf{w} \in \overline{\mathbb{PC}}_\mathbf{w} \mid \|\mathbf{w}(t)\| \leq \rho_\mathbf{w} \ \forall\ t \in \mathbb{R}\}$ with $\rho_\mathbf{w} > 0$. To define the class of systems considered in the ESC problem setting, we give the following definition of so-called convergent systems, which we have adopted from [27].

Definition 1 ([27, Sec. 2.2.1]): A system of the form $\dot{\mathbf{x}} = \mathbf{F}(\mathbf{x}, t)$, where $\mathbf{x} \in \mathbb{R}^{n_\mathbf{x}}$, $t \in \mathbb{R}$, and $\mathbf{F}(\mathbf{x}, t)$ locally Lipschitz in $\mathbf{x}$ and piecewise continuous in t, is said to be: 1) convergent in a set $\mathcal{X} \subset \mathbb{R}^{n_\mathbf{x}}$ if there exists a solution $\bar{\mathbf{x}}(t)$, called the steady-state solution, satisfying the following conditions—$\bar{\mathbf{x}}(t)$ is defined and bounded for all $t \in \mathbb{R}$ and $\bar{\mathbf{x}}(t)$ is asymptotically stable in $\mathcal{X}$; 2) uniformly convergent in $\mathcal{X}$ if it is convergent in $\mathcal{X}$ and $\bar{\mathbf{x}}(t)$ is uniformly asymptotically stable in $\mathcal{X}$; and 3) exponentially convergent in $\mathcal{X}$ if it is convergent in $\mathcal{X}$ and $\bar{\mathbf{x}}(t)$ is exponentially stable in $\mathcal{X}$. If the system is convergent in $\mathcal{X} = \mathbb{R}^{n_\mathbf{x}}$, then it is called globally convergent.

From Definition 1, we have that if the system is globally uniformly convergent, then there exists a $\mathcal{KL}$-function $\beta(r, s)$ such that any solution $\mathbf{x}(t)$ of the system satisfies

$$\|\mathbf{x}(t) - \bar{\mathbf{x}}(t)\| \leq \beta(\|\mathbf{x}(t_0) - \bar{\mathbf{x}}(t_0)\|, t - t_0). \tag{2}$$

The time-dependence of the right-hand side of the system $\dot{\mathbf{x}} = \mathbf{F}(\mathbf{x}, t)$ can often be attributed to some time-varying input, for example, a disturbance. Therefore, the next definition defines the convergence property for systems with inputs.

Definition 2 ([27, Sec. 2.2.2]): A system of the form $\dot{\mathbf{x}} = \mathbf{F}(\mathbf{x}, \mathbf{v}(t))$, with state $\mathbf{x} \in \mathbb{R}^{n_\mathbf{x}}$, input $\mathbf{v} \in \mathbb{R}^{n_\mathbf{v}}$, and $\mathbf{F}(\mathbf{x}, \mathbf{v})$ locally Lipschitz in $\mathbf{x}$ and continuous in $\mathbf{v}$, is said to be (uniformly, exponentially) convergent in $\mathcal{X} \subset \mathbb{R}^{n_\mathbf{x}}$ for a class of inputs $\mathcal{V} \subset \overline{\mathbb{PC}}_\mathbf{v}$ if it is (uniformly, exponentially) convergent in $\mathcal{X}$ for every input $\mathbf{v}(\cdot) \in \mathcal{V}$. In order to emphasize the dependence of the steady-state solution on the input $\mathbf{v}(t)$, it is denoted by $\bar{\mathbf{x}}_\mathbf{v}(t)$.

We adopt the following assumption on the system in (1) (see [14]).

Assumption 1: The nonlinear system Σ_p in (1) is globally uniformly exponentially convergent for a class of disturbances $\mathbf{w}(\cdot) \in \mathcal{W}$ and for all constant input $\mathbf{u} \in \mathbb{R}^{n_\mathbf{u}}$, uniformly in $\mathbf{u}$. In addition, given a disturbance $\mathbf{w} \in \mathcal{W}$, the globally exponentially stable (GES) steady-state solution, which we denote by $\bar{\mathbf{x}}_\mathbf{w}(t, \mathbf{u})$, is twice continuously differentiable in $\mathbf{u}$ and satisfies

$$\left\| \frac{\partial \bar{\mathbf{x}}_\mathbf{w}}{\partial \mathbf{u}}(t, \mathbf{u}) \right\| \leq L_{\mathbf{xu}} \tag{3}$$

for all $t \in \mathbb{R}$, all $\mathbf{u} \in \mathbb{R}^{n_\mathbf{u}}$, and some constant $L_{\mathbf{xu}} \in \mathbb{R}_{>0}$.

Given Assumption 1, for constant inputs $\mathbf{u} \in \mathbb{R}^{n_\mathbf{u}}$ and a given $\mathbf{w} \in \mathcal{W}$, there exists a unique, time-varying steady-state output of the system Σ_p in (1), denoted by $\bar{\mathbf{e}}_\mathbf{w}(t, \mathbf{u})$, which is given by

$$\bar{\mathbf{e}}_\mathbf{w}(t, \mathbf{u}) = \mathbf{g}(\bar{\mathbf{x}}_\mathbf{w}(t, \mathbf{u}), \mathbf{u}, \mathbf{w}(t)). \tag{4}$$

The aim is to find constant inputs $\mathbf{u}$ that optimize the steady-state performance of the system in (1). Common practice (in the ESC literature) is to define a cost function in terms of the system responses and inputs that quantify the performance of interest for the system under study. For example, consider the following performance measure, which is adopted from [12]:

$$L_2(t, \mathbf{e}(t)) := \frac{1}{T} \int_{t-T}^{t} \|\mathbf{e}(\tau)\|^2 d\tau \quad \forall t \geq T \tag{5}$$

where $T \in \mathbb{R}_{>0}$ typically indicates a known performance relevant time interval. In the case where, for constant inputs $\mathbf{u}$, the steady-state plant outputs $\bar{\mathbf{e}}_\mathbf{w}$ in (4) are *constant* or *periodic* with period time T, the steady-state output of the cost function in (5) is constant as well. Having a constant steady-state output of the cost function for constant inputs $\mathbf{u}$ is one of the basis requirements in the ESC literature that studies the data-based optimization of stable (nonlinear) systems by means of ESC (see [12], [23], [38]). However, in many (industrial) applications, this requirement is not met, as the steady-state plant outputs $\bar{\mathbf{e}}_\mathbf{w}(t, \mathbf{u})$ that characterize system performance are generically *time-varying* in nature (also for constant $\mathbf{u}$). In addition, periodicity of the steady-state plant outputs $\bar{\mathbf{e}}_\mathbf{w}$ is not evident due to the fact that system responses can be induced by complex, time-varying, possibly nonperiodic disturbances and reference trajectories. In those cases, often the neighborhood to which the ESC scheme converges can not be made arbitrarily small, thereby limiting the achievable performance gain.

2) Dynamic Cost Function $Z + \Sigma_f$: To deal with the time-varying nature of the system responses, Hazeleger *et al.* [13], [14] proposed the series connection of the system Σ_p as in (1), and a so-called dynamic cost function, i.e., the series connection of a cost function Z of the form

$$y(t) = Z(\mathbf{e}(t), \mathbf{u}(t)) \tag{6}$$

where $y \in \mathbb{R}$, and a user-defined filter, denoted by Σ_f, which has the following general form:

$$\Sigma_f : \begin{cases} \dot{\mathbf{z}}(t) = \alpha_\mathbf{z} \mathbf{h}(\mathbf{z}(t), y(t)) \\ l(t) = k(\mathbf{z}(t)) \end{cases} \tag{7}$$

where $\alpha_\mathbf{z} \in \mathbb{R}_{>0}$ is a tuning parameter, $\mathbf{z} \in \mathbb{R}^{n_\mathbf{z}}$ is the state of the filter, $y \in \mathbb{R}$ is the input of the filter defined by (6), and

$l \in \mathbb{R}$ is the output of the filter. The function $Z : \mathbb{R}^{n_\mathbf{e}} \times \mathbb{R}^{n_\mathbf{u}} \to \mathbb{R}$ is designed to be twice continuously differentiable with respect to both arguments. Moreover, we choose Z in such a way that there exist constants $L_{Z\mathbf{e}}$, $L_{Z\mathbf{u}} \in \mathbb{R}_{>0}$ such that

$$\left\| \frac{\partial^2 Z}{\partial \mathbf{e} \partial \mathbf{e}^\top}(\mathbf{e}, \mathbf{u}) \right\| \leq L_{Z\mathbf{e}}, \quad \left\| \frac{\partial^2 Z}{\partial \mathbf{e} \partial \mathbf{u}^\top}(\mathbf{e}, \mathbf{u}) \right\| \leq L_{Z\mathbf{u}} \tag{8}$$

for all $\mathbf{e} \in \mathbb{R}^{n_\mathbf{e}}$ and all $\mathbf{u} \in \mathbb{R}^{n_\mathbf{u}}$. Given a disturbance $\mathbf{w} \in \mathcal{W}$, for all constant inputs $\mathbf{u} \in \mathbb{R}^{n_\mathbf{u}}$, the steady-state output of Z is denoted by $\bar{y}_\mathbf{w}(t, \mathbf{u})$ and reads

$$\bar{y}_\mathbf{w}(t, \mathbf{u}) = Z(\mathbf{g}(\bar{\mathbf{x}}_\mathbf{w}(t, \mathbf{u}), \mathbf{u}, \mathbf{w}(t)), \mathbf{u}). \tag{9}$$

The design of the dynamic cost function should satisfy the following property.

Property 1: The dynamic cost function consisting of the cascade of Z and Σ_f, given by (6) and (7), respectively, is exponentially input-to-state convergent[1] for all constant inputs $\mathbf{u} \in \mathbb{R}^{n_\mathbf{u}}$ and all $\alpha_\mathbf{z} \in \mathbb{R}_{>0}$, uniformly in $\mathbf{u}$.

Instead of defining system performance in a time-averaged sense as in (5) with fixed period time T, the filter Σ_f is introduced to act as an averaging operator on $y(t)$ in (6), which quantifies system performance similar to the use of exponentially weighting filters [1], [41]. By tuning $\alpha_\mathbf{z}$ sufficiently small, the solution $\mathbf{z}(t)$ will vary "slowly" in time, i.e., the output of the filter $l(t)$ will be quasi-constant and determined predominantly by the average of $y(t)$. By properly designing cost function Z and tuning $\alpha_\mathbf{z}$ in (7) small, the output of the dynamic cost function $l(t)$ is quasi-constant and reflects the performance of the system while being characterized by the time-varying system response $\mathbf{e}(t)$. Hence, by subsequently minimizing $l(t)$ using ESC, we optimize the time-varying system response $\mathbf{e}(t)$.

3) Extended Plant Dynamics Σ: The series connection of the nonlinear plant Σ_p in (1) and the dynamic cost function, consisting of the cost function Z in (6) and filter Σ_f in (7), is referred to as the extended plant Σ and is schematically shown in Fig. 1. The dynamics of the extended plant is given by

$$\Sigma : \begin{cases} \dot{\mathbf{x}}(t) = \mathbf{f}(\mathbf{x}(t), \mathbf{u}(t), \mathbf{w}(t)) \\ \dot{\mathbf{z}}(t) = \alpha_\mathbf{z} \mathbf{h}(\mathbf{z}(t), Z(\mathbf{g}(\mathbf{x}(t), \mathbf{u}(t), \mathbf{w}(t)), \mathbf{u}(t))) \\ l(t) = k(\mathbf{z}(t)). \end{cases} \tag{10}$$

By similar arguments as in [27, Proof of Property 2.27], we can conclude from Assumption 1 and Property 1 that the extended plant Σ is globally uniformly exponentially convergent for a class of disturbances $\mathbf{w}(\cdot) \in \mathcal{W}$, for all constant inputs $\mathbf{u} \in \mathbb{R}^{n_\mathbf{u}}$, uniformly in $\mathbf{u}$. This implies that there exists a unique steady-state solution of Σ_f, denoted by $\bar{\mathbf{z}}_\mathbf{w}(t, \mathbf{u}, \alpha_\mathbf{z})$ and induced by the extended plant, which is defined and bounded on $t \in \mathbb{R}$ and GES. We denote this steady-state solution by $\bar{\mathbf{z}}_\mathbf{w}(t, \mathbf{u}, \alpha_\mathbf{z})$ to emphasize the dependence on time-varying disturbances $\mathbf{w}(t)$, constant inputs $\mathbf{u}$, and the tunable parameter $\alpha_\mathbf{z}$.

[1]For details on input-to-state convergent systems, see [27, Sec. 2.2.2.].

4) Parameter-to-Steady-State Performance Map: Next, we define the objective function $F_\mathbf{w}$ in terms of the steady-state solution $\bar{\mathbf{z}}_\mathbf{w}$ of the extended plant Σ, for which we adopt part of [14, Assumption 11].

Assumption 2: Given a disturbance $\mathbf{w}(t) \in \mathcal{W}$, there exists a twice continuously differentiable function $\mathbf{q}_\mathbf{w} : \mathbb{R}^{n_\mathbf{u}} \to \mathbb{R}^{n_\mathbf{z}}$, referred to as the constant performance cost, such that

$$\mathbf{q}_\mathbf{w}(\mathbf{u}) = \lim_{\alpha_\mathbf{z} \to 0} \bar{\mathbf{z}}_\mathbf{w}(t, \mathbf{u}, \alpha_\mathbf{z}) \tag{11}$$

for all $t \in \mathbb{R}$, and all $\mathbf{u} \in \mathbb{R}^{n_\mathbf{u}}$. Moreover, there exist constants $\delta_{\mathbf{z}1}, \delta_{\mathbf{z}2} \in \mathbb{R}_{\geq 0}$, related to the disturbance $\mathbf{w}(t)$ and the extended plant Σ, such that the difference between the steady-state solution $\bar{\mathbf{z}}_\mathbf{w}(t, \mathbf{u}, \alpha_\mathbf{z})$ and the function $\mathbf{q}_\mathbf{w}(\mathbf{u})$ satisfies

$$\|\bar{\mathbf{z}}_\mathbf{w}(t, \mathbf{u}, \alpha_\mathbf{z}) - \mathbf{q}_\mathbf{w}(\mathbf{u})\| \leq \alpha_\mathbf{z}\big(\delta_{\mathbf{z}1} + \delta_{\mathbf{z}2}\|\mathbf{u} - \mathbf{u}_\mathbf{w}^*\|^2\big) \tag{12}$$

for all $t \in \mathbb{R}$, all $\mathbf{u} \in \mathbb{R}^{n_\mathbf{u}}$, and all $0 < \alpha_\mathbf{z} \leq \epsilon_\mathbf{z}$ for some constant $\epsilon_\mathbf{z} \in \mathbb{R}_{>0}$, where $\mathbf{u}_\mathbf{w}^*$ denotes the optimal vector of tunable system parameters.

Hence, by Assumption 2, under steady-state conditions of the extended plant dynamics in (10), the limit $\alpha_\mathbf{z} \to 0$, and for constant inputs $\mathbf{u}$, we have that the parameter-to-steady-state performance map of the system can be characterized as follows:

$$F_\mathbf{w}(\mathbf{u}) := k(\mathbf{q}_\mathbf{w}(\mathbf{u})) \quad \forall\, \mathbf{u} \in \mathbb{R}^{n_\mathbf{u}}. \tag{13}$$

We have adopted the following assumption on $F_\mathbf{w}$ in (13) from [14].

Assumption 3: Given a disturbance $\mathbf{w} \in \mathcal{W}$, the objective function $F_\mathbf{w} : \mathbb{R}^{n_\mathbf{u}} \to \mathbb{R}$ in (13) is twice continuously differentiable and exhibits a unique minimum in $\mathbb{R}^{n_\mathbf{u}}$. Let the corresponding optimal input $\mathbf{u}_\mathbf{w}^*$ be defined as $\mathbf{u}_\mathbf{w}^* := \arg\min_{\mathbf{u} \in \mathbb{R}^{n_\mathbf{u}}} F_\mathbf{w}(\mathbf{u})$. There exist constants $L_{F1}, L_{F2} \in \mathbb{R}_{>0}$ such that

$$\frac{dF_\mathbf{w}}{d\mathbf{u}}(\mathbf{u} - \mathbf{u}_\mathbf{w}^*) \geq L_{F1}\|\mathbf{u} - \mathbf{u}_\mathbf{w}^*\|^2, \quad \left\| \frac{d^2 F_\mathbf{w}}{d\mathbf{u} d\mathbf{u}^\top} \right\| \leq L_{F2} \tag{14}$$

for all $\mathbf{u} \in \mathbb{R}^{n_\mathbf{u}}$.

To optimize the time-varying system behavior $\bar{\mathbf{e}}_\mathbf{w}$, we aim to find the system parameter values $\mathbf{u}$ for which the objective function in (13) is minimal. Information of the objective function can only be obtained through measured outputs l of the extended plant in (10). On the basis of these measured outputs, we aim to steer the inputs $\mathbf{u}$ to their performance-optimizing values $\mathbf{u}_\mathbf{w}^*$ by using the measured extended plant output $l(t)$ as feedback to an extremum-seeking controller that is introduced next.

B. Extremum-Seeking Controller

The extremum-seeking controller employed in this article is based on the one in [11, Ch. 2]. A novel ESC design extension will be presented in Section II-C. We will briefly elaborate on: 1) the dither signal design; 2) a model of the input–output behavior of the extended plant to be used as a basis for gradient estimation; 3) a least-squares observer to estimate the state of the model (and therewith the gradient of the objective function $F_\mathbf{w}$); and 4) a normalized optimizer to steer the system parameters $\mathbf{u}$ to the minimizer $\mathbf{u}_\mathbf{w}^*$.

1) Dither Signal: In order to estimate the gradient of the objective function $F_{\mathbf{w}}$ and use this estimated gradient to drive $\mathbf{u}$ toward $\mathbf{u}_{\mathbf{w}}^*$ by an optimizer, we supply the following dither signal:

$$\mathbf{u}(t) = \hat{\mathbf{u}}(t) + \alpha_{\boldsymbol{\omega}}\boldsymbol{\omega}(t) \tag{15}$$

where $\alpha_{\boldsymbol{\omega}}\boldsymbol{\omega}$ is a vector of perturbation signals with amplitude $\alpha_{\boldsymbol{\omega}} \in \mathbb{R}_{>0}$ and $\hat{\mathbf{u}}$ is referred to as the nominal system parameter to be generated by the extremum-seeking controller. The vector $\boldsymbol{\omega}$ is defined by $\boldsymbol{\omega}(t) = [\omega_1(t), \omega_2(t), \ldots, \omega_{n_{\mathbf{u}}}(t)]^\top$, with

$$\omega_i(t) = \begin{cases} \sin\left(\frac{i+1}{2}\eta_{\boldsymbol{\omega}} t\right), & \text{if } i \text{ is odd} \\ \cos\left(\frac{i}{2}\eta_{\boldsymbol{\omega}} t\right), & \text{if } i \text{ is even} \end{cases} \tag{16}$$

for $i = \{1, 2, \ldots, n_{\mathbf{u}}\}$, where $\eta_{\boldsymbol{\omega}} \in \mathbb{R}_{>0}$ is a tuning parameter.

2) Model of Input–Output Behavior of the Extended Plant: To obtain an estimate of the gradient of the objective function (13), the input-to-output behavior of the extended plant in (10), that is, from input $\hat{\mathbf{u}}$ to measured output l, is modeled in a general form. We define the state vector of the model as

$$\mathbf{m}(t) = \begin{bmatrix} F_{\mathbf{w}}(\hat{\mathbf{u}}(t)) \\ \alpha_{\boldsymbol{\omega}} \dfrac{dF_{\mathbf{w}}}{d\mathbf{u}^\top}(\hat{\mathbf{u}}(t)) \end{bmatrix}. \tag{17}$$

The measured output of the extended plant l in (10) can be written as

$$l(t) = r(t) + F_{\mathbf{w}}(\mathbf{u}(t)) + d(t) \tag{18}$$

with the signals $r(t)$ and $d(t)$ defined as

$$\begin{aligned} r(t) &:= k(\mathbf{z}(t)) - k(\bar{\mathbf{z}}_{\mathbf{w}}(t, \mathbf{u}(t), \alpha_{\mathbf{z}})) \\ d(t) &:= k(\bar{\mathbf{z}}_{\mathbf{w}}(t, \mathbf{u}(t), \alpha_{\mathbf{z}})) - k(\mathbf{q}_{\mathbf{w}}(\mathbf{u}(t))). \end{aligned} \tag{19}$$

Using Taylor's theorem and (15), the objective function $F_{\mathbf{w}}$ can be written as

$$\begin{aligned} F_{\mathbf{w}}(\mathbf{u}(t)) = F_{\mathbf{w}}(\hat{\mathbf{u}}(t)) &+ \alpha_{\boldsymbol{\omega}} \frac{dF_{\mathbf{w}}}{d\mathbf{u}}(\hat{\mathbf{u}}(t))\boldsymbol{\omega}(t) \\ &+ \frac{1}{2}\alpha_{\boldsymbol{\omega}}^2 \boldsymbol{\omega}^\top(t)\mathbf{H}(t, \hat{\mathbf{u}}(t))\boldsymbol{\omega}(t) \end{aligned} \tag{20}$$

where $\mathbf{H}(t, \hat{\mathbf{u}}(t))$ reads

$$\mathbf{H}(t, \hat{\mathbf{u}}(t)) = 2\int_0^1 (1-\sigma)\frac{d^2 F_{\mathbf{w}}}{d\mathbf{u} d\mathbf{u}^\top}(\hat{\mathbf{u}}(t) + \sigma\alpha_{\boldsymbol{\omega}}\boldsymbol{\omega}(t))d\sigma. \tag{21}$$

The dynamics of the state vector in (17) is governed by

$$\begin{aligned} \dot{\mathbf{m}}(t) &= \mathbf{A}(t)\mathbf{m}(t) + \alpha_{\boldsymbol{\omega}}^2 \mathbf{B}\mathbf{s}(t) \\ l(t) &= \mathbf{C}(t)\mathbf{m}(t) + \alpha_{\boldsymbol{\omega}}^2 \upsilon(t) + r(t) + d(t) \end{aligned} \tag{22}$$

with the matrices $\mathbf{A}$, $\mathbf{B}$, and $\mathbf{C}$ defined as

$$\begin{aligned} \mathbf{A}(t) &= \frac{1}{\alpha_{\boldsymbol{\omega}}}\begin{bmatrix} 0 & \dot{\hat{\mathbf{u}}}^\top(t) \\ \mathbf{0}^{n_{\mathbf{u}}\times 1} & \mathbf{0}^{n_{\mathbf{u}}\times n_{\mathbf{u}}} \end{bmatrix}, \quad \mathbf{B} = \begin{bmatrix} \mathbf{0}^{1\times n_{\mathbf{u}}} \\ \mathbf{I}^{n_{\mathbf{u}}\times n_{\mathbf{u}}} \end{bmatrix} \\ \mathbf{C}(t) &= \begin{bmatrix} 1 & \boldsymbol{\omega}^\top(t) \end{bmatrix} \end{aligned} \tag{23}$$

and the signals $\mathbf{s}(t)$ and $\upsilon(t)$ defined as follows:

$$\mathbf{s}(t) := \frac{d^2 F_{\mathbf{w}}}{d\mathbf{u} d\mathbf{u}^\top}(\hat{\mathbf{u}}(t))\frac{\dot{\hat{\mathbf{u}}}(t)}{\alpha_{\boldsymbol{\omega}}}, \quad \upsilon(t) := \frac{1}{2}\boldsymbol{\omega}^\top(t)\mathbf{H}(t, \hat{\mathbf{u}}(t))\boldsymbol{\omega}(t). \tag{24}$$

The signals $\mathbf{s}$, υ, r, and d can be interpreted as unknown disturbances to the model in (22). The influences of $\mathbf{s}$, υ, r, and d on the state and output of the model in (22) are small: 1) if $\hat{\mathbf{u}}$ is slowly time varying, 2) if $\alpha_{\boldsymbol{\omega}}$ is small; 3) if the states $\mathbf{x}$ of the system in (1) and the states $\mathbf{z}$ of the filter in (7) are close to their steady-state values, respectively, $\bar{\mathbf{x}}_{\mathbf{w}}$ and $\bar{\mathbf{z}}_{\mathbf{w}}$, and 4) if $\alpha_{\mathbf{z}}$ is sufficiently small.

3) Controller Design: The state $\mathbf{m}$ in (17) contains the gradient of the objective function, scaled by the perturbation amplitude $\alpha_{\boldsymbol{\omega}}$. Hence, an estimate of the gradient of the objective function $F_{\mathbf{w}}$ can be obtained from an estimate of the state $\mathbf{m}$. Here, we present a least-squares observer to estimate the state $\mathbf{m}$ of the model in (22) based on the measured outputs of the extended plant $l(t)$. The least-squares observer, denoted by Σ_o, is given by

$$\Sigma_o : \begin{cases} \dot{\hat{\mathbf{m}}} = \left(\mathbf{A} - \eta_{\mathbf{m}}\sigma_r \mathbf{Q}\mathbf{D}^\top\mathbf{D}\right)\hat{\mathbf{m}} + \alpha_{\boldsymbol{\omega}}^2 \mathbf{B}\hat{\mathbf{s}} \\ \quad + \eta_{\mathbf{m}}\mathbf{Q}\mathbf{C}^\top(l - \mathbf{C}\hat{\mathbf{m}} - \alpha_{\boldsymbol{\omega}}^2\hat{\upsilon}) \\ \dot{\mathbf{Q}} = \eta_{\mathbf{m}}\mathbf{Q} + \mathbf{A}\mathbf{Q} + \mathbf{Q}\mathbf{A}^\top \\ \quad - \eta_{\mathbf{m}}\mathbf{Q}(\mathbf{C}^\top\mathbf{C} + \sigma_r\mathbf{D}^\top\mathbf{D})\mathbf{Q} \end{cases} \tag{25}$$

with initial conditions $\hat{\mathbf{m}}(0) = \hat{\mathbf{m}}_0 \in \mathbb{R}^{n_{\mathbf{u}}+1}$ and $\mathbf{Q}(0) = \mathbf{Q}_0 \in \mathbb{R}^{n_{\mathbf{u}}+1\times n_{\mathbf{u}}+1}$, where $\mathbf{Q}_0$ is a symmetric and positive definite matrix, $\mathbf{D} = [\mathbf{0}^{n_{\mathbf{u}}\times 1} \;\; \mathbf{I}^{n_{\mathbf{u}}\times n_{\mathbf{u}}}]$, $\eta_{\mathbf{m}} \in \mathbb{R}_{>0}$ and $\sigma_r \in \mathbb{R}_{\geq 0}$ are tuning parameters related to the observer, referred to as a forgetting factor and a regularization constant, respectively, and signals $\hat{\mathbf{s}}$ and $\hat{\upsilon}$ are defined as

$$\hat{\mathbf{s}} := \hat{\mathbf{H}}(t, \hat{\mathbf{u}}(t))\frac{\dot{\hat{\mathbf{u}}}(t)}{\alpha_{\boldsymbol{\omega}}}, \quad \hat{\upsilon} := \frac{1}{2}\boldsymbol{\omega}^\top(t)\hat{\mathbf{H}}(t, \hat{\mathbf{u}}(t))\boldsymbol{\omega}(t) \tag{26}$$

with a user-defined function $\hat{\mathbf{H}} : \mathbb{R} \times \mathbb{R}^{n_{\mathbf{u}}} \to \mathbb{R}^{n_{\mathbf{u}}\times n_{\mathbf{u}}}$ satisfying $\|\hat{\mathbf{H}}(t, \hat{\mathbf{u}})\| \leq L_{\mathbf{H}}$, for all $t \in \mathbb{R}$, all $\hat{\mathbf{u}} \in \mathbb{R}^{n_{\mathbf{u}}}$, and with $L_{\mathbf{H}} \in \mathbb{R}_{>0}$. Note that in order to arrive at the observer design in (25), we have considered the signals r and d in (22) to be negligibly small. The optimizer, denoted by Σ_r, uses the estimated gradient to steer the nominal system inputs $\hat{\mathbf{u}}$ to their performance optimal values $\mathbf{u}_{\mathbf{w}}^*$. The optimizer Σ_r is given by

$$\Sigma_r : \;\; \dot{\hat{\mathbf{u}}}(t) = -\lambda_{\mathbf{u}} \frac{\eta_{\mathbf{u}}\mathbf{D}\hat{\mathbf{m}}(t)}{\eta_{\mathbf{u}} + \lambda_{\mathbf{u}}\|\mathbf{D}\hat{\mathbf{m}}(t)\|} \tag{27}$$

with $\lambda_{\mathbf{u}}$, $\eta_{\mathbf{u}} \in \mathbb{R}_{>0}$ being tuning parameters related to the optimizer.

C. Modified ESC Design for Enhanced Convergence Speed

The least-squares observer presented in Section II-B, used to obtain a local estimate of the gradient of the objective function $F_{\mathbf{w}}$, is constructed based on a general model of the input–output behavior of the extended plant in (10), that is, from input $\hat{\mathbf{u}}$ to measured output l. To be able to obtain an accurate gradient estimate of $F_{\mathbf{w}}(\hat{\mathbf{u}})$, on the one hand, the user-defined filter Σ_f must act on a slow enough time scale to reduce the effect of time-varying behavior in the steady-state output of the filter l, leading to a quasi-static approximation of the objective function $F_{\mathbf{w}}(\hat{\mathbf{u}})$. On the other hand, for this quasi-static approximation of $F_{\mathbf{w}}(\hat{\mathbf{u}})$ to hold in case of dithering, the perturbation of the input $\hat{\mathbf{u}}$ must be even slower. As a result, convergence of the ESC scheme is generally slow.

The convergence speed of the ESC scheme can be improved by increasing the frequency of the perturbation as it allows for a larger optimizer gain. However, this can lead to a deterioration of the gradient estimation because the quasi-static approximation of $F_{\mathbf{w}}(\hat{\mathbf{u}}(t))$, in the case of high-frequency perturbations, is distorted by the dynamics of the filter Σ_f. Instead, by considering the dynamics of the user-defined filter Σ_f in the observer design, this distortion of quasi-static approximation can be considered, improving the convergence speed in cases where the time scales of the perturbation and filter are similar. We propose an alternative least-squares observer design that incorporates user-defined filters Σ_f of the LTI type, which enables enhanced convergence speed of the resulting ESC scheme. We revisit the model of the input–output behavior with knowledge on Σ_f and provide the modified ESC design. In Section II-E, the effectiveness of the modified ESC design is shown using a simulation example.

1) Model of Input–Output Behavior With Knowledge on Σ_f: The model presented here extends the model in Section II-B. Let us focus on LTI designs of the filter Σ_f in (7), given by the following form:

$$\Sigma_f : \begin{cases} \dot{\mathbf{z}}(t) = \alpha_{\mathbf{z}}\big(\mathbf{A}_{\Sigma_f}\mathbf{z}(t) + \mathbf{B}_{\Sigma_f} y(t)\big) \\ l(t) = \mathbf{C}_{\Sigma_f}\mathbf{z}(t) \end{cases} \tag{28}$$

with the matrices $\mathbf{A}_{\Sigma_f} \in \mathbb{R}^{n_{\mathbf{z}}\times n_{\mathbf{z}}}$, $\mathbf{B}_{\Sigma_f} \in \mathbb{R}^{n_{\mathbf{z}}\times 1}$, and $\mathbf{C}_{\Sigma_f} \in \mathbb{R}^{1\times n_{\mathbf{z}}}$. Note that if $\mathbf{A}_{\Sigma_f}$ is Hurwitz, then Σ_f is exponentially stable, and Property 1 is guaranteed. Let us define a state $\mathbf{m}_{\mathbf{z}}$ governed by the following dynamics:

$$\dot{\mathbf{m}}_{\mathbf{z}} = \alpha_{\mathbf{z}}\big(\mathbf{A}_{\Sigma_f}\mathbf{m}_{\mathbf{z}}(t) + \mathbf{B}_{\Sigma_f} F_{\mathbf{w}}(\mathbf{u}(t))\big) \tag{29}$$

where $\mathbf{m}_{\mathbf{z}} \in \mathbb{R}^{n_{\mathbf{z}}}$. We can reformulate the output l in (28) as follows:

$$l(t) = \mathbf{C}_{\Sigma_f}\mathbf{m}_{\mathbf{z}}(t) + \mathbf{C}_{\Sigma_f}\tilde{\mathbf{m}}_{\mathbf{z}}(t) \tag{30}$$

where $\tilde{\mathbf{m}}_{\mathbf{z}} := \mathbf{z} - \mathbf{m}_{\mathbf{z}}$, and generated by the following dynamics:

$$\dot{\tilde{\mathbf{m}}}_{\mathbf{z}} = \alpha_{\mathbf{z}}\big(\mathbf{A}_{\Sigma_f}\tilde{\mathbf{m}}_{\mathbf{z}}(t) + \mathbf{B}_{\Sigma_f}(y(t) - F_{\mathbf{w}}(\mathbf{u}(t)))\big). \tag{31}$$

We can define a new state vector, which reads

$$\mathbf{m}_f^\top = \begin{bmatrix} \mathbf{m}_{\mathbf{z}}^\top & \mathbf{m}^\top \end{bmatrix}^\top \in \mathbb{R}^{n_{\mathbf{m}_f}} \tag{32}$$

with $n_{\mathbf{m}_f} = n_{\mathbf{z}} + n_{\mathbf{u}} + 1$. By using (29), (20), and the dynamics of the state vector $\mathbf{m}$ in (22), the dynamics governing the state vector in (32) is given as follows:

$$\begin{aligned} \dot{\mathbf{m}}_f(t) &= \mathbf{A}_f(t)\mathbf{m}_f(t) + \alpha_{\boldsymbol{\omega}}^2\mathbf{B}_f\mathbf{s}(t) + \alpha_{\mathbf{z}}\alpha_{\boldsymbol{\omega}}^2\mathbf{E}_f v(t) \\ l(t) &= \mathbf{C}_f\mathbf{m}_f(t) + \mathbf{C}_{\Sigma_f}\tilde{\mathbf{m}}_{\mathbf{z}}(t) \end{aligned} \tag{33}$$

with the matrices $\mathbf{A}_f \in \mathbb{R}^{n_{\mathbf{m}_f}\times n_{\mathbf{m}_f}}$, $\mathbf{B}_f \in \mathbb{R}^{n_{\mathbf{m}_f}\times n_{\mathbf{u}}}$, $\mathbf{C}_f \in \mathbb{R}^{1\times n_{\mathbf{m}_f}}$, and $\mathbf{E}_f \in \mathbb{R}^{n_{\mathbf{m}_f}\times 1}$, which are defined as follows:

$$\begin{aligned} \mathbf{A}_f(t) &= \begin{bmatrix} \alpha_{\mathbf{z}}\mathbf{A}_{\Sigma_f} & \alpha_{\mathbf{z}}\mathbf{B}_{\Sigma_f} & \alpha_{\mathbf{z}}\mathbf{B}_{\Sigma_f}\boldsymbol{\omega}^\top(t) \\ \mathbf{0}^{1\times n_{\mathbf{z}}} & 0 & \dfrac{\hat{\mathbf{u}}^\top}{\alpha_{\boldsymbol{\omega}}} \\ \mathbf{0}^{n_{\mathbf{u}}\times n_{\mathbf{z}}} & 0^{n_{\mathbf{u}}\times 1} & \mathbf{0}^{n_{\mathbf{u}}\times n_{\mathbf{u}}} \end{bmatrix} \\ \mathbf{B}_f^\top &= \begin{bmatrix} \mathbf{0}^{n_{\mathbf{u}}\times n_{\mathbf{z}}} & \mathbf{0}^{n_{\mathbf{u}}\times 1} & \mathbf{I}^{n_{\mathbf{u}}\times n_{\mathbf{u}}} \end{bmatrix} \\ \mathbf{C}_f &= \begin{bmatrix} \mathbf{C}_{\Sigma_f} & 0 & \mathbf{0}^{1\times n_{\mathbf{u}}} \end{bmatrix} \\ \mathbf{E}_f^\top &= \begin{bmatrix} \mathbf{B}_{\Sigma_f}^\top & 0 & \mathbf{0}^{1\times n_{\mathbf{u}}} \end{bmatrix}. \end{aligned} \tag{34}$$

2) Controller Design With Knowledge on Σ_f: Inspired by the observer in (25), the least-squares observer to estimate $\mathbf{m}_f$ of the model in (33), denoted by Σ_{fo}, is given by

$$\Sigma_{fo} : \begin{cases} \dot{\hat{\mathbf{m}}}_f = \big(\mathbf{A}_f - \eta_{\mathbf{m}}\sigma_r\mathbf{Q}_f\mathbf{D}_f^\top\mathbf{D}_f\big)\hat{\mathbf{m}}_f + \alpha_{\boldsymbol{\omega}}^2\mathbf{B}_f\hat{\mathbf{s}} \\ \quad +\alpha_{\mathbf{z}}\alpha_{\boldsymbol{\omega}}^2\mathbf{E}_f\hat{v} + \eta_{\mathbf{m}}\mathbf{Q}_f\mathbf{C}_f^\top(l - \mathbf{C}_f\hat{\mathbf{m}}_f) \\ \dot{\mathbf{Q}}_f = \eta_{\mathbf{m}}\mathbf{Q}_f + \mathbf{A}_f\mathbf{Q}_f + \mathbf{Q}_f\mathbf{A}_f^\top \\ \quad -\eta_{\mathbf{m}}\mathbf{Q}_f(\mathbf{C}_f^\top\mathbf{C}_f + \sigma_r\mathbf{D}_f^\top\mathbf{D}_f)\mathbf{Q}_f \end{cases} \tag{35}$$

with initial conditions $\hat{\mathbf{m}}_f(0) = \hat{\mathbf{m}}_{f0} \in \mathbb{R}^{n_{\mathbf{m}_f}}$ and $\mathbf{Q}_f(0) = \mathbf{Q}_{f0} \in \mathbb{R}^{n_{\mathbf{m}_f}\times n_{\mathbf{m}_f}}$, where $\mathbf{Q}_{f0}$ is a symmetric and positive definite matrix, and the matrix $\mathbf{D}_f$ defined as

$$\mathbf{D}_f = [\mathbf{0}^{n_{\mathbf{u}}\times n_{\mathbf{z}}} \quad \mathbf{0}^{n_{\mathbf{u}}\times 1} \quad \mathbf{I}^{n_{\mathbf{u}}\times n_{\mathbf{u}}}]. \tag{36}$$

The signals $\hat{\mathbf{s}}$ and $\hat{v}$ are defined in (26). To arrive at the observer design in (35), we have assumed $\tilde{\mathbf{m}}_{\mathbf{z}}$ to be negligibly small, similar to the signals r and d in the observer design in (25). Again, this is justified for steady-state conditions of the extended plant Σ and sufficiently small $\alpha_{\mathbf{z}}$. The optimizer, denoted by Σ_{fr}, reads as follows:

$$\Sigma_{fr} : \quad \dot{\hat{\mathbf{u}}}(t) = -\lambda_{\mathbf{u}}\frac{\eta_{\mathbf{u}}\mathbf{D}_f\hat{\mathbf{m}}_f(t)}{\eta_{\mathbf{u}} + \lambda_{\mathbf{u}}\big\|\mathbf{D}_f\hat{\mathbf{m}}_f(t)\big\|}. \tag{37}$$

D. Stability Analysis

Next, we provide a stability result and supporting stability proof for the closed-loop ESC scheme with the modified extremum-seeking controller proposed in Section II-C. The next result states the conditions on tuning parameters under which the ESC scheme with the modified extremum-seeking controller guarantees that $\hat{\mathbf{u}}$ converges to an arbitrarily small set around the optimum $\mathbf{u}_{\mathbf{w}}^*$.

Theorem 1: Consider a (time-varying) disturbance $\mathbf{w} \in \mathcal{W}$ and Assumptions 1–3 and [14, Assumption 1]. Moreover, consider arbitrary initial conditions $\mathbf{x}(0) \in \mathbb{R}^{n_{\mathbf{x}}}$ and $\mathbf{Q}_f(0) \in \mathbb{R}^{n_{\mathbf{m}_f}\times n_{\mathbf{m}_f}}$ symmetric and positive definite, $\hat{\mathbf{u}}(0) \in \mathcal{U}_0$, with $\mathcal{U}_0 \subset \mathbf{R}^{n_{\mathbf{u}}}$ an arbitrary large compact subset, $\mathbf{z}(0) \in \mathbb{R}^{n_{\mathbf{z}}}$, and $\hat{\mathbf{m}}_f(0) \in \mathbb{R}^{n_{\mathbf{m}_f}}$. Then, there exist (sufficiently small) constants $\epsilon_0, \ldots, \epsilon_5 \in \mathbb{R}_{>0}$, such that, for all tunable parameters $\alpha_{\mathbf{z}}, \alpha_{\boldsymbol{\omega}}, \eta_{\mathbf{u}}, \lambda_{\mathbf{u}}, \eta_{\mathbf{m}}, \eta_{\boldsymbol{\omega}} \in \mathbb{R}_{>0}$ and $\sigma_r \in \mathbb{R}_{\geq 0}$ with $\alpha_{\boldsymbol{\omega}} \leq \epsilon_0$, $\eta_{\boldsymbol{\omega}} \leq \alpha_{\mathbf{z}}\epsilon_1$, $\alpha_{\mathbf{z}} \leq \eta_{\mathbf{m}}\epsilon_2$, $\alpha_{\boldsymbol{\omega}}\lambda_{\mathbf{u}} \leq \eta_{\mathbf{m}}\epsilon_3$, $\eta_{\mathbf{u}} \leq \alpha_{\boldsymbol{\omega}}\eta_{\boldsymbol{\omega}}\epsilon_4$, and $\sigma_r \leq \epsilon_5$, the solutions of the closed-loop system consisting of the extended plant in (10) and the modified extremum-seeking controller [consisting of the dither signal in (15), the observer Σ_{fo} in (35), and the optimizer Σ_{fr} in (37)] are bounded for all $t \geq 0$. In addition, there exist constants $c_1, \ldots, c_5 \in \mathbb{R}_{>0}$ such that the solutions $\hat{\mathbf{u}}(t)$ satisfy

$$\begin{aligned} \limsup_{t\to\infty} \|\hat{\mathbf{u}}(t) - \mathbf{u}_{\mathbf{w}}^*\| \leq \max\Bigg\{ &\alpha_{\boldsymbol{\omega}}\eta_{\boldsymbol{\omega}}^2\, c_1, \alpha_{\mathbf{z}}\alpha_{\boldsymbol{\omega}}\delta_{\mathbf{z}2}c_2, \\ &\eta_{\boldsymbol{\omega}}c_3, \frac{\alpha_{\mathbf{z}}}{\alpha_{\boldsymbol{\omega}}}c_4\delta_{\mathbf{z}1}, \alpha_{\boldsymbol{\omega}}c_5 \Bigg\}. \end{aligned} \tag{38}$$

Proof 1: The proof of Theorem 1 follows similar arguments as in [11, Proof of Theorem 2.8] and [14, Proof of Theorem 14]. Different from [14, Th. 14], the proofs are the bounds on the solutions of the error

dynamics of the novel least-squares observer in (35). Here, we will present these bounds. Let us introduce the following coordinate transformation:

$$\begin{aligned}\tilde{\mathbf{m}}_f(t) &= \hat{\mathbf{m}}_f(t) - \mathbf{m}_f(t)\\ \tilde{\mathbf{Q}}_f(t) &= \mathbf{Q}_f^{-1}(t) - \Xi_f^{-1}\end{aligned} \tag{39}$$

with $\Xi_f^{-1} = \mathbf{C}_f^\top \mathbf{C}_f + \sigma_r \mathbf{D}_f^\top \mathbf{D}_f$. From the observer in (35), the coordinate transformation in (39), and the model of the input–output behavior in (33), we have the following state equations for $\tilde{\mathbf{Q}}_f$ and $\tilde{\mathbf{m}}_f$:

$$\dot{\tilde{\mathbf{Q}}}_f = -\eta_{\mathbf{m}}\tilde{\mathbf{Q}}_f - \Xi_f^{-1}\mathbf{A}_f - \mathbf{A}_f^\top \Xi_f^{-1} - \tilde{\mathbf{Q}}_f\mathbf{A}_f - \mathbf{A}_f^\top\tilde{\mathbf{Q}}_f \tag{40}$$

$$\begin{aligned}\dot{\tilde{\mathbf{m}}}_f = &\left(\mathbf{A}_f - \eta_{\mathbf{m}}\mathbf{Q}_f(\mathbf{C}_f^\top\mathbf{C}_f + \sigma_r\mathbf{D}_f^\top\mathbf{D}_f)\right)\tilde{\mathbf{m}}_f\\ &+\alpha_\omega^2\mathbf{B}_f(\hat{\mathbf{s}} - \mathbf{s}) - \eta_{\mathbf{m}}\sigma_r\alpha_\omega\mathbf{Q}_f\mathbf{D}_f^\top\frac{dF_{\mathbf{w}}}{d\mathbf{u}^\top}(\hat{\mathbf{u}})\\ &+\alpha_{\mathbf{z}}\alpha_\omega^2\mathbf{E}_f(\hat{v} - v) + \eta_{\mathbf{m}}\mathbf{Q}_f\mathbf{C}_f^\top\mathbf{C}_{\Sigma_f}\tilde{\mathbf{m}}_{\mathbf{z}}.\end{aligned} \tag{41}$$

Note that we have omitted most arguments of the variables in (40) and (41) for notational clarity. First, a bound on the solutions $\tilde{\mathbf{Q}}_f(t)$ is presented in Lemma 1.

Lemma 1: For any $\epsilon_1, \epsilon_4 \in \mathbb{R}_{>0}$, sufficiently small $\epsilon_2, \epsilon_5 \in \mathbb{R}_{>0}$, and all tunable parameters $\alpha_\omega, \eta_{\mathbf{m}} \in \mathbb{R}_{>0}$, there exist constants $c_{\mathbf{Q}}$, $\beta_{\mathbf{Q}} \in \mathbb{R}_{>0}$ such that, for all $\eta_\omega \leq \alpha_{\mathbf{z}}\epsilon_1$, $\alpha_{\mathbf{z}} \leq \eta_{\mathbf{m}}\epsilon_2$, all $\eta_{\mathbf{u}} \leq \alpha_\omega\eta_\omega\epsilon_4$, and all $\sigma_r \leq \epsilon_5$, the solutions $\tilde{\mathbf{Q}}_f$ satisfy

$$\|\tilde{\mathbf{Q}}_f(t)\| \leq \max\left\{c_{\mathbf{Q}}\|\tilde{\mathbf{Q}}_f(0)\|e^{-\eta_{\mathbf{m}}\beta_{\mathbf{Q}}t}, \frac{1}{8}\right\} \tag{42}$$

for all $t \geq 0$, all $\tilde{\mathbf{Q}}_f(0) \in \mathbb{R}^{n_{\mathbf{m}_f}\times n_{\mathbf{m}_f}}$ for which $\mathbf{Q}_f(0)$ is symmetric and positive definite, and all time-varying $\mathbf{u}(t) \in \mathbb{R}^{n_{\mathbf{u}}}$.

Proof 2: See Appendix A. □

Second, a bound on the solutions $\tilde{\mathbf{m}}_f(t)$ for time-varying inputs $\mathbf{u}(t)$ is presented in Lemma 2.

Lemma 2: For any $\epsilon_0, \epsilon_1, \epsilon_2, \epsilon_4 \in \mathbb{R}_{>0}$, sufficiently small $\epsilon_5 \in \mathbb{R}_{>0}$, any finite time $t_1 \geq 0$, and any $\delta_{\mathbf{z}1}$, $\delta_{\mathbf{z}2} \in \mathbb{R}_{\geq 0}$, the solutions $\tilde{\mathbf{m}}_f$ are bounded for all $0 \leq t \leq t_1$, all $\tilde{\mathbf{u}}(0) \in \mathbb{R}^{n_{\mathbf{u}}}$, all $\tilde{\mathbf{m}}_f(0) \in \mathbb{R}^{n_{\mathbf{m}_f}}$, all $\alpha_\omega \leq \epsilon_0, \eta_\omega \leq \alpha_{\mathbf{z}}\epsilon_1, \alpha_{\mathbf{z}} \leq \eta_{\mathbf{m}}\epsilon_2, \eta_{\mathbf{u}} \leq \alpha_\omega\eta_\omega\epsilon_4$, and all $\sigma_r \leq \epsilon_5$. In addition, for sufficiently small $\epsilon_3, \epsilon_5 \in \mathbb{R}_{>0}$ and all $\alpha_\omega\lambda_{\mathbf{u}} \leq \eta_{\mathbf{m}}\epsilon_3$, there exist constants $c_{\mathbf{m}1}, \ldots, c_{\mathbf{m}8}(\epsilon_0), \ldots, c_{\mathbf{m}10}(\epsilon_2) \in \mathbb{R}_{>0}$ such that the solutions $\tilde{\mathbf{m}}_f$ satisfy

$$\begin{aligned}\sup_{t\geq t_1}\|\tilde{\mathbf{m}}_f(t)\| \leq \sup_{t\geq t_1}\max\Big\{&c_{\mathbf{m}1}\|\tilde{\mathbf{m}}_f(t_1)\|, \sqrt{\sigma_r}\alpha_\omega c_{\mathbf{m}2}\|\tilde{\mathbf{u}}(t)\|\\ &\alpha_\omega\frac{\alpha_\omega\lambda_{\mathbf{u}}}{\eta_{\mathbf{m}}}c_{\mathbf{m}3}\|\tilde{\mathbf{u}}(t)\|, \alpha_{\mathbf{z}}c_{\mathbf{m}4}\delta_{\mathbf{z}2}\|\tilde{\mathbf{u}}(t)\|^2, \alpha_\omega\eta_\omega c_{\mathbf{m}5}\|\tilde{\mathbf{u}}(t)\|\\ &\alpha_\omega^2\eta_\omega^2\ c_{\mathbf{m}6}, \alpha_{\mathbf{z}}\alpha_\omega^2\ c_{\mathbf{m}7}\delta_{\mathbf{z}2}, \alpha_\omega\eta_\omega c_{\mathbf{m}8}, \alpha_{\mathbf{z}}c_{\mathbf{m}9}\delta_{\mathbf{z}1}, \alpha_\omega^2 c_{\mathbf{m}10}\Big\}\end{aligned} \tag{43}$$

$$\begin{aligned}\limsup_{t\to\infty}\|\tilde{\mathbf{m}}_f(t)\| \leq \limsup_{t\to\infty}\max\Big\{&\sqrt{\sigma_r}\alpha_\omega c_{\mathbf{m}2}\|\tilde{\mathbf{u}}(t)\|\\ &\alpha_\omega\frac{\alpha_\omega\lambda_{\mathbf{u}}}{\eta_{\mathbf{m}}}c_{\mathbf{m}3}\|\tilde{\mathbf{u}}(t)\|, \alpha_{\mathbf{z}}c_{\mathbf{m}4}\delta_{\mathbf{z}2}\|\tilde{\mathbf{u}}(t)\|^2, \alpha_\omega\eta_\omega c_{\mathbf{m}5}\|\tilde{\mathbf{u}}(t)\|\\ &\alpha_\omega^2\eta_\omega^2\ c_{\mathbf{m}6}, \alpha_{\mathbf{z}}\alpha_\omega^2\ c_{\mathbf{m}7}\delta_{\mathbf{z}2}, \alpha_\omega\eta_\omega c_{\mathbf{m}8}, \alpha_{\mathbf{z}}c_{\mathbf{m}9}\delta_{\mathbf{z}1}, \alpha_\omega^2 c_{\mathbf{m}10}\Big\}.\end{aligned} \tag{44}$$

Proof 3: See Appendix B. □

On the basis of [14, Proof of Theorem 14] and the bounds on the solutions $\tilde{\mathbf{Q}}_f(t)$ and $\tilde{\mathbf{m}}_f(t)$ in Lemmas 1 and 2, respectively, we obtain the bounds on the solutions $\hat{\mathbf{u}}(t) - \mathbf{u}_{\mathbf{w}}^*$ in (38), which completes the proof of Theorem 1. □

Remark 1: (Tuning Guidelines): Under the conditions of Theorem 1, it follows that if we are dealing with constant (or no) disturbances $\mathbf{w}$, i.e., $\delta_{\mathbf{z}1}, \delta_{\mathbf{z}2} = 0$ (see Assumption 2), the optimizer state $\hat{\mathbf{u}}$ converges to an arbitrarily small region of the performance optimal value $\mathbf{u}_{\mathbf{w}}^*$ if the dither parameters α_ω and η_ω are chosen sufficiently small for an arbitrary bounded $\alpha_{\mathbf{z}}$. Choosing $\alpha_{\mathbf{z}}$ large in general allows faster convergence toward the performance optimal value $\mathbf{u}_{\mathbf{w}}^*$. In the case of time-varying disturbances $\mathbf{w}(t)$, i.e., $\delta_{\mathbf{z}1}, \delta_{\mathbf{z}2} > 0$, we subsequently tune α_ω small to make the fifth term in the right-hand side of (38) arbitrarily small, tune $\alpha_{\mathbf{z}}$ small to make the second and fourth term arbitrarily small, and finally tune η_ω small to make the first and third terms arbitrarily small.

E. Illustrative Example: Enhanced Convergence Speed

To illustrate the enhanced convergence speed of the modified extremum-seeking controller, we have adopted the following exemplary dynamical system from [12]:

$$\Sigma_p: \begin{cases}\dot{x}_1(t) = x_2(t)\\ \dot{x}_2(t) = -25x_1(t) - b(u(t))x_2(t) + w(t)\\ e(t) = x_1(t)\end{cases} \tag{45}$$

where $b(u) = 10 + 5(u-10)^2$ is a nonlinear characteristic that depends on the system input $u \in \mathbb{R}$ and $w(t) = 20\sin(2\pi\, 10\, t)$ is an input disturbance. In this example, the aim is to find the input u that maximizes[2] the amplitude of the steady-state output of the system in (45) given the particular disturbance $w(t)$. Note that, for each constant input u, the system in (45) is a GES linear system subject to external inputs $w(t)$, which implies that it is globally exponentially convergent, thereby satisfying Assumption 1. We employ the following dynamic cost function, with cost function $Z: y(t) = e(t)^2$, and filter Σ_f given by a low-pass filter $\dot{z}(t) = \alpha_{\mathbf{z}}(y(t) - z(t))$, $l(t) = z(t)$, with $\alpha_{\mathbf{z}}$ the cutoff frequency. Here, we employ both ESC strategies given by (25)–(27) and (35)–(37), respectively, to investigate the effect of including information of the user-designed filter Σ_f in the observer on the convergence speed. For both extremum-seeking controllers, we employ the following numerical values: $\alpha_\omega = 0.25$, $\eta_\omega = 4$, $\eta_{\mathbf{m}} = 2$, $\lambda_{\mathbf{u}} = 1.5\times10^6$, $\eta_{\mathbf{u}} = 0.75$, $\sigma_r = 1\times10^{-3}$, and $\hat{\mathbf{H}} = -5\times10^{-7}$. Moreover, we show the results for both extremum-seeking controllers with two filter settings: $\alpha_{\mathbf{z}} = 3$ and $\alpha_{\mathbf{z}} = 10$.

Fig. 2 shows the simulation results that show the convergence of the initial input $u(0) = 3$ to a small neighborhood of the optimal input $u_{\mathbf{w}}^* = 10$ for both filter settings $\alpha_{\mathbf{z}} = 3$ and $\alpha_{\mathbf{z}} = 10$ and both the nominal ESC design, and the modified ESC design. For all settings, it can seen that the input u

[2]The extremum-seeking controllers presented in this section are designed for minimization problems. Without loss of generality, we can employ the same controllers for maximization problems by changing the sign of the cost function.

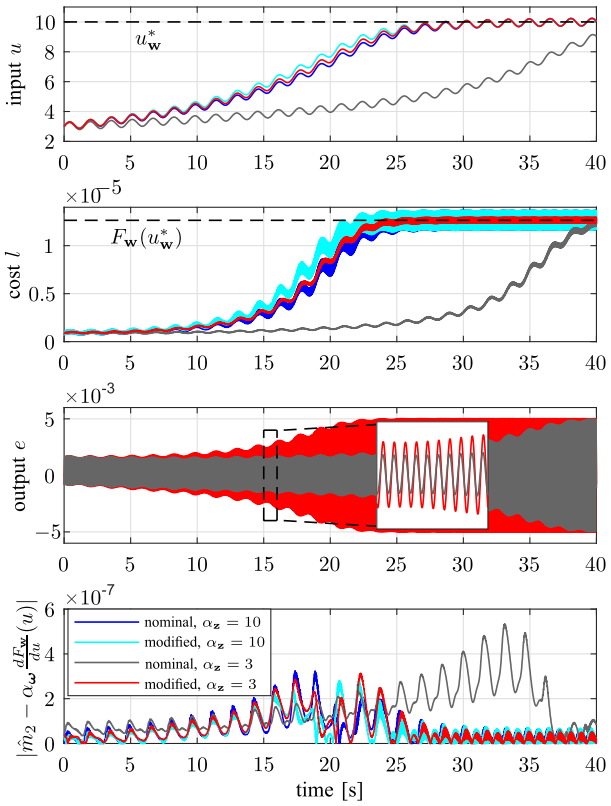

Fig. 2. Simulation results of both extremum-seeking controllers. By incorporation knowledge on the filter in the observer, we achieve faster convergence toward the optimal input $u^*_{\mathbf{w}} = 10$ (top). The improved convergence of the modified controller is more significant in cases where the value of $\alpha_{\mathbf{z}}$ is relatively small.

converges toward $u^*_{\mathbf{w}}$ (top), and the amplitude of the output e increases (third subfigure).

In addition, Fig. 2 shows the improved convergence speed as a result of incorporating knowledge about Σ_f. For $\alpha_{\mathbf{z}} = 3$, the modified case (red) shows a significantly faster convergence toward $u^*_{\mathbf{w}}$ than the nominal case (gray). The bottom subfigure in Fig. 2 shows the state estimation error $|\hat{m}_2 - \alpha_{\boldsymbol{\omega}}(dF_{\mathbf{w}}/du)(u)|$, where $\hat{m}_i$ denotes, on the one hand, the ith element of state vector $\hat{\mathbf{m}}$ in the nominal case (gray), and on the other hand, the $(i+1)$th element of state vector $\hat{\mathbf{m}}_f$ in the modified case (red). In the modified case, it can be seen that, overall, the estimation of the gradient of $F_{\mathbf{w}}$ is improved compared to the gradient obtained with the nominal ESC design. The modified ESC design considers the dynamics of the filter and, thus, the distortion of the filter on the perturbation with $\eta_{\boldsymbol{\omega}} = 4$ and its effect on the quasi-constant output of the extended plant, which leads to the improved convergence speed of the modified extremum-seeking controller. In case of $\alpha_{\mathbf{z}} = 10$, the convergence speed in the nominal case (blue plots in the first and second subfigures) is marginally improved compared to the convergence speed in the modified case (cyan plots in the first and second subfigures). Concluding, in the presence of time-varying steady-state plant responses, in cases where slow filter dynamics are used in combination with a relatively fast dither signal, the modified extremum-seeking controller outperforms the nominal case in terms of convergence speed.

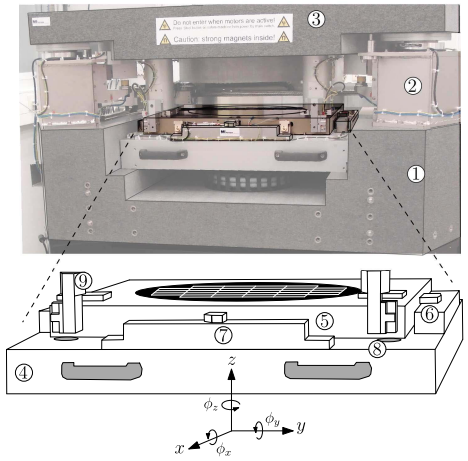

Fig. 3. Industrial motion stage setup. ① Base frame. ② Airmounts. ③ Metrology frame. ④ Force frame. ⑤ Chuck. ⑥ x-direction actuators. ⑦ y-direction actuators. ⑧ z-direction actuators. ⑨ sensors.

III. Industrial Motion Stage Setup and Performance Optimization Problem Formulation

In this section, we will give a brief description of the industrial motion stage setup under study and its nonlinear feedback control design. The motion stage setup (see Fig. 3) represents the short-stroke motion of a wafer stage commonly found in, e.g., complex lithography machinery used to manufacture integrated circuits (ICs) (for more details, see [4]). Wafer stages are required to perform fast (re)positioning in three degrees of freedom with *nm*-accuracy to achieve the desired high machine throughput. Achieving *nm*-accuracy and high speeds of the wafer stage is in general realized by high-gain linear feedback controllers. However, due to the well-known waterbed effect (see [7]), increasing the gain further to improve the ability to suppress low-frequency disturbances comes at the expense of increased sensitivity to high-frequency disturbances and noise. Instead, on the basis of a dead-zone nonlinearity and the error signal, VGC can schedule an additional gain.

Although VGC is intuitive in nature, performance optimal tuning of a variable-gain controller depends heavily on the (unknown) disturbance situation at hand. In Section IV, we will use the motion stage setup with VGC to experimentally demonstrate both the nominal and the modified ESC approach for the optimization of time-varying steady-state responses.

A. System Description

The industrial motion stage setup, shown in Fig. 3, consist of a base frame ① which is directly connected to the fixed world, force actuators in x-, y-, and z-directions, respectively, ⑥, ⑦, and ⑧, which are installed in a force frame ④ that rests on the base frame, encoders in x-, y-, and z-directions ⑨ which are connected to a metrology frame ③ that is isolated from the base frame by means of airmounts ②, and a chuck ④, supported by four passive gravity compensators at the corners ⑧ to achieve a mid-air equilibrium of the chuck. The chuck,

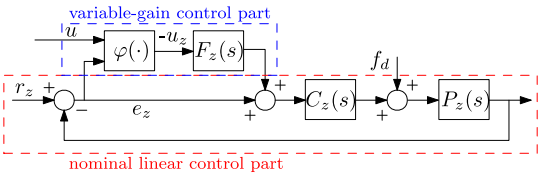

Fig. 4. Closed-loop VGC scheme.

being the main component of the setup, can be controlled in all six DOFs by means of force actuators. The origin of the reference frame is located at the center of gravity of the chuck. Lorentz actuators are used to actuate the chuck in the x-, y-, and ϕ_z-directions, and voice coil actuators are used to actuate the chuck in the ϕ_x-, ϕ_y-, and z-directions.

B. Nominal and Nonlinear Feedback Control Design

In this section, we focus on controlling the chuck in the z-direction with the (nonlinear) feedback control loop shown in Fig. 4. Here, $P_z(s)$ represents the (motion) plant dynamics of the actuated chuck (in the z-direction), with $s \in \mathbb{C}$ being the Laplace variable. The nonlinear control loop consists of two parts, namely, a nominal linear feedback control part and a VGC part. For the nominal linear feedback control part, transfer function $C_z(s)$ represents the nominal (low-gain) linear controller. The signals r_z, e_z, and f_d denote the setpoint and tracking error in the z-direction, and (external, time-varying) disturbances, respectively. Here, we consider $r_z = 0$.

For the so-called VGC part, $\varphi(\cdot)$ denotes a nonlinear control element, and transfer function $F_z(s)$ is a shaping filter. The nonlinear control element $\varphi(\cdot)$ studied here is given by a dead-zone characteristic

$$\varphi(e_z(t), u) = \begin{cases} \alpha(e_z(t) + u), & \text{if } e_z(t) < -u \\ 0, & \text{if } |e_z(t)| \leq u \\ \alpha(e_z(t) - u), & \text{if } e_z(t) > u \end{cases} \tag{46}$$

where α, $u \in \mathbb{R}_{\geq 0}$ are tunable parameters, referred to as the additional gain and the dead-zone length, respectively. From the nonlinearity in (46), we can identify three distinct cases.

1) For $u = \infty$, the output of the nonlinear element $\varphi(\cdot)$ is always zero; the VGC part is disabled and only the nominal, low-gain, linear controller $C_z(s)$ is active. This case is referred to as the low-gain case.
2) For $u = 0$, the nonlinear element $\varphi(\cdot)$ acts as a gain α, and the VGC part has the transfer $\alpha F_z(s)$. Effectively, this case is referred to as the high-gain case; the high-gain linear controller reads $C_z(s)(1 + \alpha F_z(s))$.
3) For $u \in (0, \infty)$, we have nonlinear behavior, where the output of nonlinear element $\varphi(\cdot)$ depends on the amplitude of the tracking error $e_z(t)$. This case is referred to as the variable-gain case.

The closed-loop dynamics of the VGC scheme shown in Fig. 4 can be written as a Lur'e-type system having the following state-space form:

$$\Sigma_p : \begin{cases} \dot{\mathbf{x}}(t) = \mathbf{A}_p \mathbf{x}(t) + \mathbf{B}_p u_z(t) + \mathbf{B}_w \mathbf{w}(t) \\ e_z(t) = \mathbf{C}_p \mathbf{x}(t) + \mathbf{D}_w \mathbf{w}(t) \\ u_z(t) = -\varphi(e_z(t), u(t)) \end{cases} \tag{47}$$

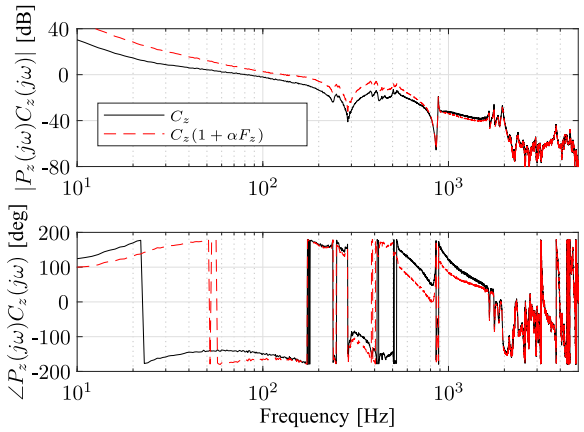

Fig. 5. Measured open-loop frequency response function with nominal, low-gain linear controller $C_z(s)$ ($u = \infty$, i.e., low-gain case), and the nominal high-gain linear controller $C_z(s)(1 + \alpha F_z(s))$ ($u = 0$, i.e., high-gain case) with the maximum allowable additional gain $\alpha = 6.48$.

with state $\mathbf{x} \in \mathbb{R}^{n_\mathbf{x}}$, and where $\mathbf{w}(t) = [r_z(t)\ f_d(t)]^\top \in \mathbb{R}^{n_\mathbf{w}}$ are all (external) disturbances. To conclude on closed-loop stability of the system in (47), we denote the transfer from u_z to e_z, i.e., from the output to the input of the nonlinear element $\varphi(\cdot)$, by the following transfer function:

$$G_{eu}(s) = \mathbf{C}_p(s\mathbf{I} - \mathbf{A}_p)^{-1}\mathbf{B}_p = \frac{P_z(s)C_z(s)F_z(s)}{1 + P_z(s)C_z(s)}. \tag{48}$$

The following theorem states the conditions under which the dynamics in (47) exhibit a unique, time-varying steady-state output that is globally uniformly exponentially stable.

Theorem 2: [40] Consider the dynamics in (47). Suppose that the following conditions hold.

1) The matrix $\mathbf{A}_p$ is Hurwitz.
2) The nonlinear element $\varphi(e_z, u)$ satisfies the so-called incremental sector condition, which reads as follows:

$$0 \leq \frac{\varphi(e_1, u) - \varphi(e_2, u)}{e_1 - e_2} \leq \alpha \tag{49}$$

for all $e_1, e_2 \in \mathbb{R}$, $e_1 \neq e_2$, and all $u \in \mathbb{R}_{\geq 0}$.
3) The transfer function $G_{eu}(s)$ in (48) satisfies the following frequency-domain condition:

$$\text{Re}\{G_{eu}(j\omega)\} > -\frac{1}{\alpha} \quad \forall\ \omega \in \mathbb{R}. \tag{50}$$

Then, for any bounded input $\mathbf{w}(t)$, the system in (47) has a unique, time-varying steady-state output which is GES.

Based on frequency response measurements of the motion stage setup, first a stabilizing linear controller $C_z(s)$ is designed using loop-shaping techniques. The linear controller $C_z(s)$, referred to as the nominal low-gain linear controller, consists of a proportional–integral–derivative (PID)-type controller, low-pass filter, and notch filters, achieving a bandwidth of 80 Hz [see the black plot in Fig. 5 for the open-loop frequency response function $P_z(j\omega)C_z(j\omega)$].

Having a stabilizing (nominal low-gain) linear controller $C_z(s)$ implies that the first condition of Theorem 2 is satisfied.

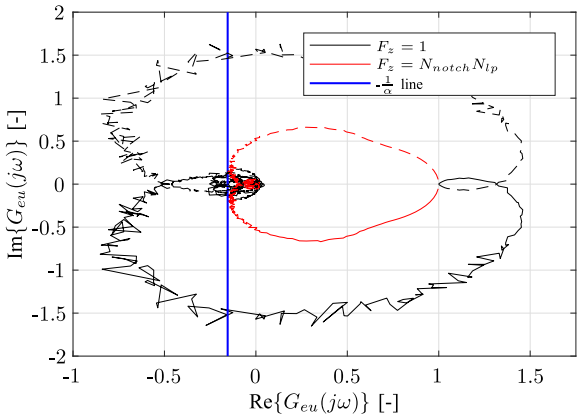

Fig. 6. Circle-criterion condition based on the measured frequency response data, verifying the satisfaction of the third condition of Theorem 2; $\mathrm{Re}\{G_{eu}(j\omega)\} > -(1/\alpha)$ for all $\omega \in \mathbb{R}$. With $F_z(s) = 1$, a maximum allowable additional gain $\alpha = 1.17$ can be achieved. With $F_z(s)$ composed of a notch filter and low-pass filter, a maximum allowable additional gain $\alpha = 6.48$ can be achieved.

Moreover, from the definition of the nonlinear element in (46) follows that the second condition of Theorem 2 is satisfied. The third condition of Theorem 2 is graphically shown in Fig. 6 and can be used to design the additional gain α of the nonlinear element in (46) and shaping filter $F_z(s)$. The shaping filter used here is given by $F_z(s) = N_{\text{notch}}(s)N_{lp}(s)$ with notch filter $N_{\text{notch}}(s)$ and the second-order low-pass filter $N_{lp}(s)$

$$N_{\text{notch}}(s) = \frac{\omega_{pN}^2}{\omega_{zN}^2}\frac{s^2 + 2\beta_{zN}\omega_{zN}s + \omega_{zN}^2}{s^2 + 2\beta_{pN}\omega_{pN}s + \omega_{pN}^2}$$
$$N_{lp}(s) = \frac{\omega_{lp}^2}{s^2 + 2\beta_{lp}\omega_{lp}s + \omega_{lp}^2} \tag{51}$$

with $\omega_{pN} = \omega_{zN} = 110 \cdot 2\pi$ rad/s, $\beta_{pN} = 3.2$, $\beta_{zN} = 0.4$, $\beta_{lp} = 1/2\sqrt{2}$, and $\omega_{lp} = 350 \cdot 2\pi$ rad/s. If we omit the shaping filter, i.e., $F_z(s) = 1$, the maximum allowable additional gain that guarantees closed-loop stability of VGC scheme is $\alpha = 1.17$. With the shaping filter $F_z(s)$ given by (51), the maximum allowable additional gain that guarantees the closed-loop stability of the VGC scheme is $\alpha = 6.48$. Having a higher additional gain α yields increased suppression of low-frequency disturbances. In addition, the low-pass filter in (51) is employed to attenuate high-frequency content of the large error signal such that the variable-gain controller does not amplify this. Fig. 5 shows the open-loop frequency response functions $P_z(j\omega)C_z(j\omega)$ for the low-gain case and high-gain case, i.e., $C_z(s)$ and $C_z(s)(1 + \alpha F_z(s))$, respectively. In the remainder, we will consider an additional gain $\alpha = 6$ for robustness purposes, which renders the closed-loop system in (47) exponentially convergent. Note that this implies the satisfaction of Assumption 1, which is a key requirement for the utilization of the proposed ESC.

C. External Disturbances

Although we consider control in the z-direction only, in industrial motion stages, the x-, y-, and z-directions are not fully decoupled. For example, in wafer scanning systems,

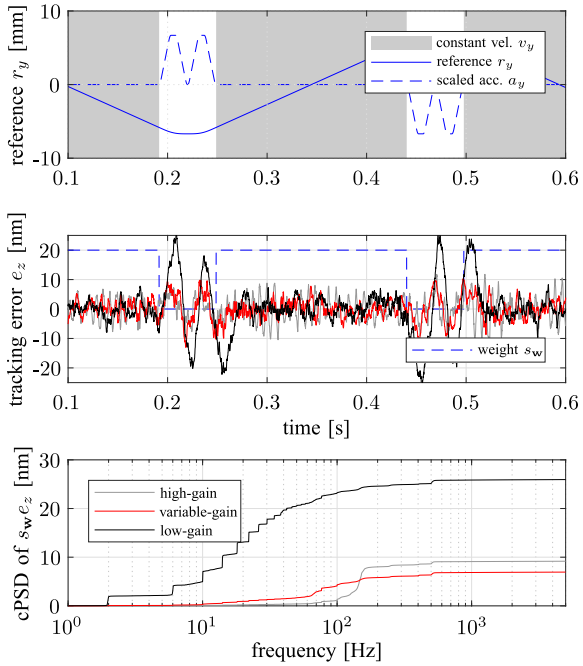

Fig. 7. Top: reference trajectory in the y-direction and a scaled acceleration profile in the y-direction. Middle: tracking error $e_z(t)$ and weighting function $s_w(t)$. Bottom: cPSD of the weighted error $s_w(t)e_z(t)$. Middle and bottom figure are for the low-, high-, and variable-gain case, with the additional gain $\alpha = 6$ and dead-zone length $u = 3$ nm.

the motion of a typical wafer stage in the x- and y-directions is usually prescribed by the third- or fourth-order reference trajectories, denoted by $r_x(t)$ and $r_y(t)$, respectively. Due to cross coupling between x-, y-, and z-axes, setpoint accelerations in the x- and y-directions, denoted by $a_x(t) := \ddot{r}_x(t)$ and $a_y(t) := \ddot{r}_y(t)$, respectively, induce low-frequency disturbances that affect the positioning accuracy in the z-direction among others. The industrial motion stage setup we consider here has a limited stroke in the x- and y-directions. In order to emulate the effect of crosstalk of these setpoint-induced disturbances to the z-direction, we inject a scaled version of the acceleration reference profile in the y-direction as an input disturbance in the z-control loop at the location where f_d enters the loop in Fig. 4. A scaled version of this acceleration profile in the y-direction can be seen in Fig. 7 (top, blue dashed plot). The gray areas denote regions where the velocity is constant, during which high-accuracy motion stage positioning in the z-direction is desired.

In addition to low-frequency disturbances induced by setpoint accelerations in the y-direction, other (high-frequency) effects are disturbing the system as well. These disturbances can be, e.g., vibrational or acoustic disturbances, measurement noise, and amplifier disturbances. Fig. 7 (middle, black plot) shows a measured tracking error in the z-direction for the low-gain case, resulting from these setpoint-induced low-frequency disturbances and other high-frequency effects.

D. System Performance Specifications

In view of the stage disturbances as discussed in Section III-C, VGC is introduced to be able to improve the ability to suppress the setpoint-induced low-frequency

disturbances in the z-direction while limiting the increased sensitivity to high-frequency disturbances under high-gain feedback. This system performance specification can be quantified by the root mean square (rms) of a weighted tracking error signal computed over a known performance relevant time interval $T = 0.498$ s. Similar to the one in (5), a typical performance measure used to quantify system performance reads

$$L_2(t, s_{\mathbf{w}}e_z(t)) := \frac{1}{T}\int_{t-T}^{t} (s_{\mathbf{w}}(\tau)e_z(\tau))^2 d\tau \quad \forall\ t \geq T \quad (52)$$

where we have introduced a weighting function $s_{\mathbf{w}}(t)$ that is defined as follows:

$$s_{\mathbf{w}}(t) = \begin{cases} 0 & \text{if } a_y(t) \neq 0 \\ 1 & \text{if } a_y(t) = 0. \end{cases} \quad (53)$$

A scaled version of the specific weighting function used here is shown in the middle plot of Fig. 7 (blue dashed plot); basically, during nonzero accelerations in the y-direction, we do not penalize the tracking error, as we are only interested in achieving improved system performance during the constant velocity phase, i.e., zero acceleration in the y-direction (see Fig. 7). Fig. 7 shows the tracking error for the low-gain case ($u = \infty$), high-gain case ($u = 0$), and the variable-gain case with $\alpha = 6$ and $u = 3 \times 10^{-9}$ m. In addition, we have depicted a plot of the cumulative power spectral density (cPSD) of the weighted tracking error and analyzed over multiple time intervals T, which shows the different frequency contributions present in the tracking error. Both plots illustrate the benefit of the variable-gain controller; we can see that, during $s_{\mathbf{w}} \neq 0$, the tracking error response e_z in the VGC case shows "the best of both worlds" in terms of the error responses in the low- and high-gain cases, that is, the variable-gain controller is able to suppress low-frequency disturbances similar to the high-gain controller, while the amplification of high-frequency disturbances, especially around 100–200 Hz, is similar to the low-gain controller.

The results in Fig. 7 show that there exists a variable-gain controller setting that outperforms the low- and high-gain cases in terms of the performance measure in (52). However, we do not know *a priori* which value for the dead-zone length u gives the best system performance, as the value of u that minimizes the performance measure in (52) depends heavily on the disturbance situation at hand. Since accurate models of the disturbance situation are difficult to obtain and the disturbance characteristic may slowly change over time, finding the optimal dead-zone length u can be difficult in practice.

In Section IV, we will show that, without explicitly using knowledge on the plant and disturbance situation at hand, we can get arbitrarily close to the optimally tuned dead-zone length u by employing the ESC approaches introduced in Section II.

IV. Experimental Results

In this section, we will present the experimental results on the performance optimal tuning of the variable-gain controller applied to the industrial motion stage setup discussed in Section III using the ESC approaches discussed in Section II. Section IV-A presents the dynamic cost function design, and Section IV-B shows the measured objective function $F_{\mathbf{w}}$ of the industrial motion stage setup given the particular disturbance situation at hand to help verify the working principles of the ESC approaches. In Sections IV-C and IV-D, measurement results are presented in the closed-loop ESC schemes with the nominal ESC design and the modified ESC design, respectively, and Section IV-E presents dedicated tuning guidelines to achieve extremum seeking for motion stages.

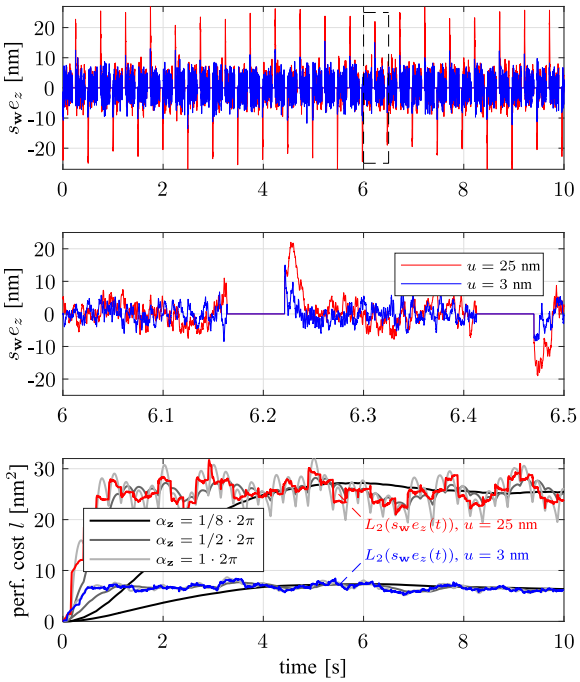

Fig. 8. Top: two measurements of the weighted tracking error with $u = 25$ nm and $u = 3$ nm against time. Middle: zoomed plot of the weighted tracking error for $t \in [6, 6.5]$. Bottom: response of the dynamic cost function l against time for different values of $\alpha_{\mathbf{z}}$, and the system performance measure in (52) for $u = 25$ nm and $u = 3$ nm.

A. Dynamic Cost Function

In order to mimic the performance measure in (52), the cost function Z in (6) is chosen as $Z:\ y(t) = (s_{\mathbf{w}}(t)e_z(t))^2$, with the weighting function $s_{\mathbf{w}}$ defined in (53), and the filter Σ_f in (7) is designed as a second-order low-pass filter with the following state-space formulation:

$$\Sigma_f : \begin{cases} \dot{z}_1(t) = \alpha_{\mathbf{z}} z_2(t) \\ \dot{z}_2(t) = \alpha_{\mathbf{z}}(y(t) - 2\beta_{\mathbf{z}} z_2(t) - z_1(t)) \\ l(t) = z_1(t) \end{cases} \quad (54)$$

with tunable parameters $\beta_{\mathbf{z}}, \alpha_{\mathbf{z}} \in \mathbb{R}_{>0}$ representing the damping coefficient and cutoff frequency of the second-order low-pass filter, respectively. The top of Fig. 8 shows two 10-s measurements of the weighted tracking error for two variable-gain cases, respectively, $u = 25$ nm (red plot) and $u = 3$ nm (blue plot). The middle of Fig. 8 shows a zoomed plot for $t \in [6, 6.5]$ s. The bottom of Fig. 8 shows the response of the dynamic cost function l for different values of $\alpha_{\mathbf{z}}$ and

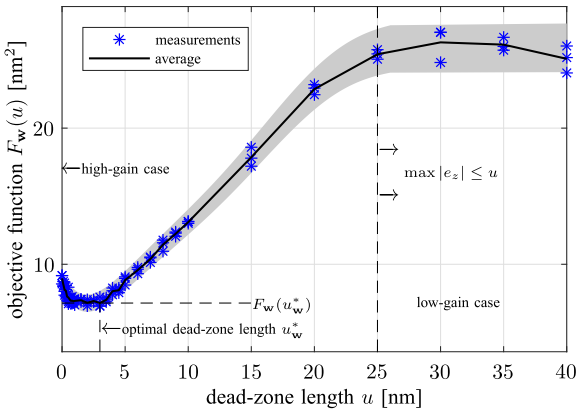

Fig. 9. Approximation of the objective function $F_{\mathbf{w}}(u)$, averaged over three measurements (10 s each) with $\alpha_{\mathbf{z}} = (1/8)\cdot 2\pi$. An average of the last 2 s of the measured performance cost l (in steady-state) is used to estimate $F_{\mathbf{w}}(u)$. The gray area indicates an area in which l approximately lies. For smaller values of $\alpha_{\mathbf{z}}$, this area becomes smaller; however, a longer measurement time is needed for the transient response to have sufficiently decayed.

the performance measure in (52) for both variable-gain cases. Clearly, the performance measure in (52) is time-varying due to the time-varying nature of the measured performance output, i.e., the weighted tracking error. The output l of the filter Σ_f approximates the performance measure in real time and is also time-varying. However, by selecting a sufficiently small $\alpha_{\mathbf{z}}$, the steady-state output, defined as $\bar{l}_{\mathbf{w}}$, can be made quasi-constant, that is, the filter Σ_f with tunable parameter $\alpha_{\mathbf{z}}$ provides robustness for the ESC scheme against the effect of time-varying system behavior on the performance measure, which can be made arbitrarily small. Note that, for smaller values of $\alpha_{\mathbf{z}}$, it takes a longer time before transient effects are sufficiently decayed. For larger $\alpha_{\mathbf{z}}$, the opposite can be concluded; the effect of time-varying system behavior on the performance measure is larger, while the transients decay faster.

B. Objective Function

The parameter-to-steady-state performance map $F_{\mathbf{w}}(u)$ [see (13)] of the industrial motion stage setup and the dynamic cost function is experimentally obtained through multiple measurements and shown in Fig. 9. The objective function clearly shows that there exists an optimal dead-zone length ($u_{\mathbf{w}} \approx 3$ nm) for this particular disturbance situation. Furthermore, the objective function shows the performance corresponding to the low-gain case ($u > 25$ nm) and high-gain case ($u = 0$ nm). The variation between the different measurements for the same dead-zone length can be attributed to multiple causes. The objective function in (13) is defined on the limit $\alpha_{\mathbf{z}} \to 0$; however, we have used $\alpha_{\mathbf{z}} = 0.25\pi$ to obtain the result in Fig. 9. As a result, the steady-state output $\bar{l}_{\mathbf{w}}$ of Σ_f is still time-varying. In addition, the external disturbances and measurement noise present during one experiment can slightly deviate from the disturbance situation during another experiment. We would like to emphasize that the objective function $F_{\mathbf{w}}(\mathbf{u})$ in Fig. 9 is typically unknown in practice, and only ESC will be used to find the optimum of $F_{\mathbf{w}}(\mathbf{u})$.

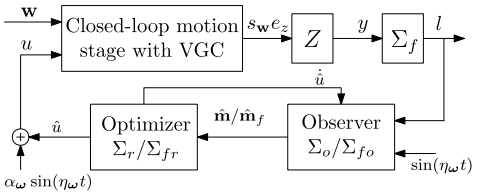

Fig. 10. Closed-loop ESC scheme composed of the closed-loop motion stage with VGC, the dynamic cost function $Z + \Sigma_f$, the observer Σ_o (or Σ_{fo}), the optimizer Σ_r (or Σ_{fr}), and the dither signal $\alpha_{\boldsymbol{\omega}}\sin(\eta_{\boldsymbol{\omega}}t)$.

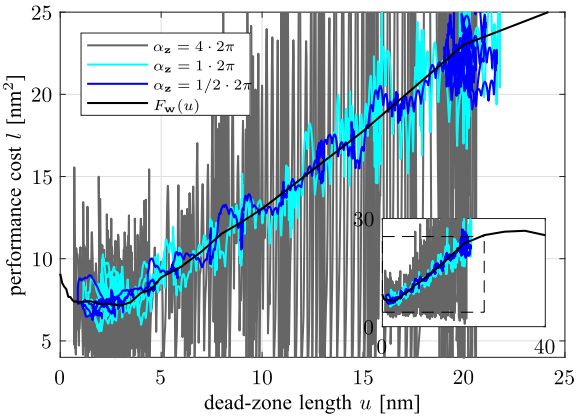

Fig. 11. Average of measured objective function $F_{\mathbf{w}}(u)$ and a plot of the measured performance cost l against the dead-zone length u for the real-time performance optimal tuning of the variable-gain controller using the nominal extremum-seeking controller and three different values of $\alpha_{\mathbf{z}}$.

TABLE I
NOMINAL EXTREMUM-SEEKING CONTROLLER SETTINGS

parameter	value	unit
dither amplitude $\alpha_{\boldsymbol{\omega}}$	0.5	[nm]
filter parameter $\alpha_{\mathbf{z}}$	$1\cdot 2\pi$	[rad/s]
dither frequency $\eta_{\boldsymbol{\omega}}$	$1/4\cdot 2\pi$	[rad/s]
damping coefficient $\beta_{\mathbf{z}}$	$(1/2)\sqrt{2}$	[-]
forgetting factor $\eta_{\mathbf{m}}$	0.5	[-]
regularization constant σ_r	$1\cdot 10^{-6}$	[-]
observer parameter $\hat{\mathbf{H}}$	0.25	[-]
optimizer parameter $\eta_{\mathbf{u}}$	$1\cdot 10^{-3}$	[-]
optimizer parameter $\lambda_{\mathbf{u}}$	$2\cdot 10^{9}$	[-]
initial condition optimizer $\hat{u}(0)$	20	[nm]
initial condition observer state $\hat{\mathbf{m}}(0)$	$[0\ 0]^\top$	[-]
initial condition observer state $\mathbf{Q}(0)$	$\begin{bmatrix} 1 & 0 \\ 0 & \frac{2}{1+2\sigma_r} \end{bmatrix}$	[-]

C. Performance Optimization Using Nominal ESC

In this section, we analyze the experimental results obtained using the ESC approaches discussed in Section II. The closed-loop ESC scheme is schematically shown in Fig. 10. The nominal settings and initial conditions of the extremum-seeking controller are shown in Table I. Figs. 11 and 12 show the convergence of the VGC parameter u starting at $u = 20$ nm toward the optimal setting $u^*_{\mathbf{w}} \approx 3$ nm, and thus the optimal system performance $F_{\mathbf{w}}(u^*_{\mathbf{w}})$, in the presence of time-varying system behavior. Moreover, the figures illustrate the convergence and the effect on the convergence speed for different values for the filter parameter $\alpha_{\mathbf{z}}$. The following observations can be made.

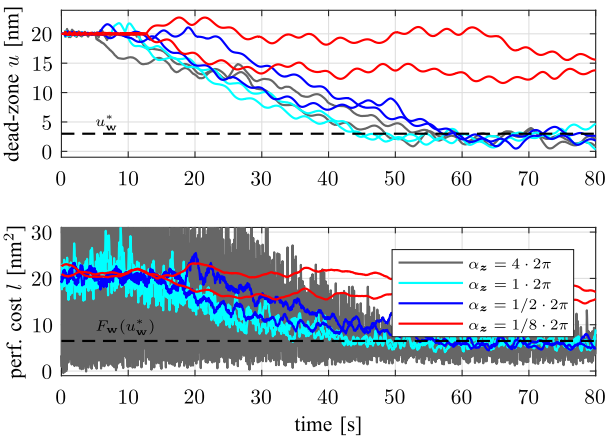

Fig. 12. Experimental results using the nominal extremum-seeking controller to illustrate the influence of $\alpha_{\mathbf{z}}$ on the convergence of the dead-zone length u toward the optimal input $u_{\mathbf{w}}^*$ and the corresponding performance cost l as a function of time. The black dashed lines indicate the optimal dead-zone length setting $u_{\mathbf{w}}^*$ (top) and the corresponding steady-state performance $F_{\mathbf{w}}(u_{\mathbf{w}}^*)$ (bottom).

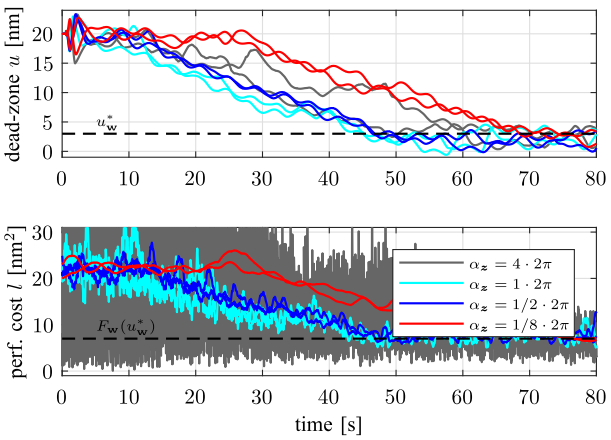

Fig. 13. Experimental results using the modified extremum-seeking controller to illustrate the influence of the tunable parameter $\alpha_{\mathbf{z}}$ on the convergence of the dead-zone length u toward the optimal input $u_{\mathbf{w}}^*$, and the corresponding performance cost l as a function of time. The black dashed lines indicate the optimal dead-zone length setting $u_{\mathbf{w}}^*$ (top) and the corresponding steady-state performance $F_{\mathbf{w}}(u_{\mathbf{w}}^*)$ (bottom).

1) Choosing a larger value for the cutoff frequency $\alpha_{\mathbf{z}}$ results in faster decay of the transient response of the filter Σ_f, which ultimately leads to faster convergence of u toward $u_{\mathbf{w}}^*$, compare, e.g., the cases $\alpha_{\mathbf{z}} = 1/2 \cdot 2\pi$ and $\alpha_{\mathbf{z}} = 1 \cdot 2\pi$. Choosing $\alpha_{\mathbf{z}}$ too high deteriorates the convergence of u toward $u_{\mathbf{w}}^*$. For example, see the "unexpected" slower convergence with $\alpha_{\mathbf{z}} = 4 \cdot 2\pi$ rad/s (gray plot) compared to the case $\alpha_{\mathbf{z}} = 1 \cdot 2\pi$ rad/s (cyan plot) in the top of Fig. 12. From the gray plot in the bottom of Fig. 12, we can see that the time-varying steady-state response of the extended plant Σ is not quasi-constant, which can lead to poor estimation of the gradient of the objective function by the observer Σ_o and, hence, a deterioration of the convergence of u toward $u_{\mathbf{w}}^*$.
2) Choosing $\alpha_{\mathbf{z}}$ too small (much smaller than the dither frequency parameterized by η_{ω}) may lead to a deterioration of the convergence of u toward $u_{\mathbf{w}}^*$ as well. For example, see the "convergence" with $\alpha_{\mathbf{z}} = 1/8 \cdot 2\pi$ rad/s in Fig. 12 (red plot). If we choose $\alpha_{\mathbf{z}}$ too low, separation between the time scales of the filter dynamics and the extremum-seeking controller is insufficient. Retuning of the extremum-seeking controller parameters, e.g., decreasing the dither frequency η_{ω}, can be necessary to preserve time-scale separation.

D. Improved Convergence Speed With Modified ESC Design

Fig. 13 shows the convergence of the VGC parameter u toward the optimal setting $u_{\mathbf{w}}^* \approx 3$ nm for the modified extremum-seeking controller. Moreover, the figure illustrates the convergence and the effect on the convergence speed for different values of the filter parameter $\alpha_{\mathbf{z}}$. The following observations can be made.

1) Similar to the nominal extremum-seeking controller, choosing a larger value for the cutoff frequency $\alpha_{\mathbf{z}}$ results in faster decay of the transient response of the filter Σ_f, which ultimately leads to faster convergence of u toward $u_{\mathbf{w}}^*$. Moreover, choosing $\alpha_{\mathbf{z}}$ too high deteriorates the convergence of u toward $u_{\mathbf{w}}^*$ (compare again the case $\alpha_{\mathbf{z}} = 4 \cdot 2\pi$ rad/s (gray plot) to the case $\alpha_{\mathbf{z}} = 1 \cdot 2\pi$ rad/s (cyan plot) in the top of Fig. 13).
2) The advantage of the modified extremum-seeking controller over the nominal one is particularly evident in case of small values of $\alpha_{\mathbf{z}}$. Where the case $\alpha_{\mathbf{z}} = 1/8 \cdot 2\pi$ rad/s led to a deterioration of the convergence of u toward $u_{\mathbf{w}}^*$ in the nominal case (see the red plot in Fig. 12), the modified extremum-seeking controller still achieves convergence to the optimal input (see the red plot in Fig. 13). In general, the improvement of the modified ESC design in terms of convergence speed is more significant in the case of smaller values of $\alpha_{\mathbf{z}}$.

The resulting optimal time-varying steady-state response $\bar{\mathbf{e}}_{\mathbf{w}}(t, \mathbf{u}_{\mathbf{w}}^*)$ can be seen in Fig. 7 (red plot).

E. Dedicated Tuning Guidelines

For the extremum-seeking controller parameters α_{ω}, $\alpha_{\mathbf{z}}$, and η_{ω}, we present some dedicated tuning guidelines when optimizing time-varying system behavior of industrial positioning stages.

1) The dither amplitude α_{ω} should be chosen close to the desired accuracy of u to the optimal VGC parameter settings $u_{\mathbf{w}}^*$ when converged, e.g., $\alpha_{\omega} = 0.5$ nm. Choosing α_{ω} small may deteriorate the convergence speed of u toward $u_{\mathbf{w}}^*$ (see Fig. 14). Choosing α_{ω} large may result in faster convergence, but the neighborhood of $u_{\mathbf{w}}^*$ to which u converges is in general larger.
2) The cutoff frequency $\alpha_{\mathbf{z}}$ of a low-pass filter design for Σ_f should typically be chosen smaller than the lowest significant frequency contribution ω_{low} in the to-be-optimized tracking error, e.g., $\alpha_{\mathbf{z}} = (1/2)\omega_{\text{low}}$. Small values of $\alpha_{\mathbf{z}}$ motivate the use of the modified extremum-seeking controller over the nominal one to prevent slow

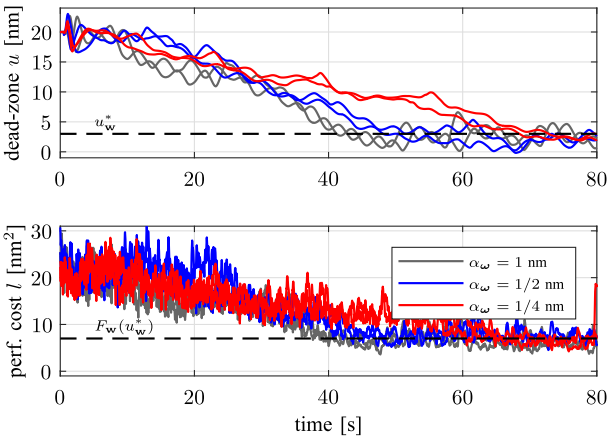

Fig. 14. Experimental results using the modified extremum-seeking controller to illustrate the influence of the dither amplitude $\alpha_{\boldsymbol{\omega}}$ on the convergence of the dead-zone length u toward the optimal input $u_{\mathbf{w}}^*$, and the corresponding performance cost l as a function of time. The black dashed lines indicate the optimal dead-zone length setting $u_{\mathbf{w}}^*$ (top) and the corresponding steady-state performance $F_{\mathbf{w}}(u_{\mathbf{w}}^*)$ (bottom).

convergence. In motion stages, the frequency ω_{low} is usually dictated by the setpoint and the performance relevant time interval T, i.e., $\omega_{\text{low}} = (2\pi/T)$.

3) The dither frequency $\eta_{\boldsymbol{\omega}}$ should be chosen close to or less than $\alpha_{\mathbf{z}}$ to have sufficient excitation and sufficient time-scale separation.

V. Conclusion

In this article, we have experimentally demonstrated the working principle and performance of an ESC approach for the optimization of time-varying responses. The experimental case study involves optimally tuning parameters of a nonlinear control strategy for an industrial motion stage setup to achieve optimal system performance. Moreover, we have proposed a modified extremum-seeking controller design that incorporates knowledge about the filter and presented a stability analysis of the closed-loop ESC scheme with the modified controller. Both simulations and experiments show that the use of the modified extremum seeking controller leads to an increased convergence speed toward the extremum, especially for small values of the dynamic cost function parameter.

Appendix A
Proof of Lemma 1

We define the following Lyapunov function candidate for the $\tilde{\mathbf{Q}}_f$-dynamics:

$$V_{\mathbf{Q}_f}(\tilde{\mathbf{Q}}_f(t)) = \text{tr}(\tilde{\mathbf{Q}}_f^2(t)). \tag{55}$$

For notational clarity, from this point on, we omit the time argument. Note that $\tilde{\mathbf{Q}}_f$ is symmetric because $\mathbf{Q}_f$ and Ξ_f^{-1} are symmetric. From (40), we can write the the time derivative of $V_{\mathbf{Q}}$ as follows:

$$\begin{aligned}\dot{V}_{\mathbf{Q}_f}(\tilde{\mathbf{Q}}_f) &= \frac{d}{dt}\text{tr}(\tilde{\mathbf{Q}}_f^2) = \text{tr}(\dot{\tilde{\mathbf{Q}}}_f\tilde{\mathbf{Q}}_f + \tilde{\mathbf{Q}}_f\dot{\tilde{\mathbf{Q}}}_f)\\ &= -2\eta_{\mathbf{m}}\text{tr}(\tilde{\mathbf{Q}}_f^2) - \text{tr}(\mathbf{A}_f^\top\Xi_f^{-1}\tilde{\mathbf{Q}}_f + \tilde{\mathbf{Q}}_f\Xi_f^{-1}\mathbf{A}_f)\\ &\quad -\text{tr}(\Xi_f^{-1}\mathbf{A}_f\tilde{\mathbf{Q}}_f + \tilde{\mathbf{Q}}_f\mathbf{A}_f^\top\Xi_f^{-1}) - 4\text{tr}(\tilde{\mathbf{Q}}_f^2\mathbf{A}_f)\end{aligned} \tag{56}$$

where we have used that $\text{tr}(\mathbf{X}+\mathbf{Y}) = \text{tr}(\mathbf{X}) + \text{tr}(\mathbf{Y})$, $\text{tr}(\mathbf{XY}) = \text{tr}(\mathbf{YX})$, and $\text{tr}(\mathbf{X}) = \text{tr}(\mathbf{X}^\top)$. From the definition of the trace, we have the following inequalities:

$$\begin{aligned}\|\tilde{\mathbf{Q}}_f\|^2 \le V_{\mathbf{Q}_f}(\tilde{\mathbf{Q}}_f) &\le n_{\mathbf{m}_f}\|\tilde{\mathbf{Q}}_f\|^2\\ \text{tr}(\tilde{\mathbf{Q}}_f^2\mathbf{A}_f) &\le n_{\mathbf{m}_f}\|\tilde{\mathbf{Q}}_f\|^2\|\mathbf{A}_f\|\\ \text{tr}(\mathbf{A}_f^\top\Xi_f^{-2}\mathbf{A}_f) &\le n_{\mathbf{m}_f}\|\Xi_f^{-1}\|^2\|\mathbf{A}_f\|^2.\end{aligned} \tag{57}$$

From (57) and the fact that $\text{tr}(\mathbf{X}^\top\mathbf{X}) \ge 0$, we obtain the following inequality:

$$\begin{aligned}\dot{V}_{\mathbf{Q}_f}(\tilde{\mathbf{Q}}_f) \le -\eta_{\mathbf{m}}V_{\mathbf{Q}_f}(\tilde{\mathbf{Q}}_f) + 4n_{\mathbf{m}_f}V_{\mathbf{Q}_f}(\tilde{\mathbf{Q}}_f)\|\mathbf{A}_f\|\\ + \frac{4}{\eta_{\mathbf{m}}}n_{\mathbf{m}_f}\|\Xi_f^{-1}\|^2\|\mathbf{A}_f\|^2.\end{aligned} \tag{58}$$

The definition of $\boldsymbol{\omega}$ in (16) implies that there exists a constant $L_{\omega 2} \in \mathbb{R}_{>0}$ such that $\|\boldsymbol{\omega}\| \le L_{\omega 2}$. Moreover, there exist $L_{\mathbf{A}_{\Sigma_f}}, L_{\mathbf{B}_{\Sigma_f}} \in \mathbb{R}_{>0}$ such that $\|\mathbf{A}_{\Sigma_f}\| \le L_{\mathbf{A}_{\Sigma_f}}$ and $\|\mathbf{B}_{\Sigma_f}\| \le L_{\mathbf{B}_{\Sigma_f}}$, respectively. From (34), we have that $\|\dot{\mathbf{A}}_f\| \le \alpha_{\mathbf{z}}(L_{\Sigma_f} + \epsilon_1\epsilon_4)$ for all $\eta_{\boldsymbol{\omega}} \le \alpha_{\mathbf{z}}\epsilon_1$, and all $\eta_{\mathbf{u}} \le \alpha_{\boldsymbol{\omega}}\eta_{\boldsymbol{\omega}}\epsilon_4$, and with $L_{\Sigma_f} := L_{\mathbf{A}_{\Sigma_f}} + L_{\mathbf{B}_{\Sigma_f}}L_{\omega 2}$. Moreover, without loss of generality, for sufficiently small ϵ_5 and a particular design of $\mathbf{C}_{\Sigma_f}$ (e.g., observable canonical form for Σ_f, such that $\|C_{\Sigma_f}\| = 1$), we have $\|\Xi_f^{-1}\| \le 2$ for all $\sigma_r \le \epsilon_5$. Using this, and without loss of generality, for sufficiently small ϵ_2 and ϵ_5, we obtain the following inequality:

$$\dot{V}_{\mathbf{Q}_f}(\tilde{\mathbf{Q}}_f) \le -\frac{\eta_{\mathbf{m}}}{2}V_{\mathbf{Q}_f}(\tilde{\mathbf{Q}}_f) + \frac{\eta_{\mathbf{m}}}{256} \tag{59}$$

for all $\eta_{\boldsymbol{\omega}} \le \alpha_{\mathbf{z}}\epsilon_1$, all $\alpha_{\mathbf{z}} \le \eta_{\mathbf{m}}\epsilon_2$, all $\eta_{\mathbf{u}} \le \alpha_{\boldsymbol{\omega}}\eta_{\boldsymbol{\omega}}\epsilon_4$, and all $\sigma_r \le \epsilon_5$. Applying the comparison lemma and using the inequalities in (57), we obtain the bound on $\tilde{\mathbf{Q}}_f$ as follows:

$$\|\tilde{\mathbf{Q}}_f(t)\| \le \max\left\{e^{-\frac{\eta_{\mathbf{m}}}{4}t}\sqrt{2\,n_{\mathbf{m}_f}}\|\tilde{\mathbf{Q}}_f(0)\|, \frac{1}{8}\right\} \tag{60}$$

for all $t \ge 0$, all $\tilde{\mathbf{Q}}_f(0) \in \mathbb{R}^{n_{\mathbf{m}_f}\times n_{\mathbf{m}_f}}$, and all time-varying $\mathbf{u}(t) \in \mathbb{R}^{n_{\mathbf{u}}}$, which completes the proof of Lemma 1. □

Appendix B
Proof of Lemma 2

We define the following Lyapunov function candidate for the $\tilde{\mathbf{m}}_f$-dynamics in (41):

$$V_{\mathbf{m}_f}(\tilde{\mathbf{m}}_f, \mathbf{Q}_f) = \tilde{\mathbf{m}}_f^\top\mathbf{Q}_f^{-1}\tilde{\mathbf{m}}_f. \tag{61}$$

For notational clarity, from this point on, we omit the time argument. We note that

$$\lambda_{\min}(\mathbf{Q}_f^{-1})\|\tilde{\mathbf{m}}_f\|^2 \le V_{\mathbf{m}_f}(\tilde{\mathbf{m}}_f, \mathbf{Q}_f) \le \lambda_{\max}(\mathbf{Q}_f^{-1})\|\tilde{\mathbf{m}}_f\|^2 \tag{62}$$

where $\lambda_{\min}(\mathbf{Q}_f^{-1})$ and $\lambda_{\max}(\mathbf{Q}_f^{-1})$ are the smallest and largest eigenvalues of $\mathbf{Q}_f^{-1}$, respectively. From the observer in (35) and (41), we obtain the time derivative of $V_{\mathbf{m}_f}$ as follows:

$$\begin{aligned}\dot{V}_{\mathbf{m}_f} &= 2\tilde{\mathbf{m}}_f^\top\mathbf{Q}_f^{-1}\dot{\tilde{\mathbf{m}}}_f - \tilde{\mathbf{m}}_f^\top\mathbf{Q}_f^{-1}\dot{\mathbf{Q}}_f\mathbf{Q}_f^{-1}\tilde{\mathbf{m}}_f\\ &= -\eta_{\mathbf{m}}\tilde{\mathbf{m}}_f^\top\mathbf{Q}_f^{-1}\tilde{\mathbf{m}}_f - \eta_{\mathbf{m}}\tilde{\mathbf{m}}_f^\top(\mathbf{C}_f^\top\mathbf{C}_f + \sigma_r\mathbf{D}_f^\top\mathbf{D}_f)\tilde{\mathbf{m}}_f\\ &\quad +2\alpha_{\boldsymbol{\omega}}^2\tilde{\mathbf{m}}_f^\top\mathbf{Q}_f^{-1}\mathbf{B}_f(\hat{\mathbf{s}} - \mathbf{s}) - 2\eta_{\mathbf{m}}\sigma_r\alpha_{\boldsymbol{\omega}}\tilde{\mathbf{m}}_f^\top\mathbf{D}_f^\top\frac{dF_{\mathbf{w}}}{d\mathbf{u}^\top}(\hat{\mathbf{u}})\\ &\quad +2\alpha_{\mathbf{z}}\alpha_{\boldsymbol{\omega}}^2\tilde{\mathbf{m}}_f^\top\mathbf{Q}_f^{-1}\mathbf{E}_f(\hat{v} - v) + 2\eta_{\mathbf{m}}\tilde{\mathbf{m}}_f^\top\mathbf{C}_f^\top\mathbf{C}_{\Sigma_f}\tilde{\mathbf{m}}_{\mathbf{z}}\end{aligned} \tag{63}$$

where we have used the fact that $\mathbf{Q}_f^{-1}$ is real and symmetric, i.e., $\mathbf{Q}_f^{-1} = \mathbf{Q}_f^{-\top}$, and, given $\mathbf{A}_f$ in (34), that $\tilde{\mathbf{m}}_f^\top(\mathbf{Q}_f^{-1}\mathbf{A}_f - \mathbf{A}_f^\top\mathbf{Q}_f^{-1})\tilde{\mathbf{m}}_f = 0$. Furthermore, given $\mathbf{C}_f$ and $\mathbf{D}_f$, using the fact that $-\tilde{\mathbf{m}}_f^\top\mathbf{C}_f^\top\mathbf{C}_f\tilde{\mathbf{m}}_f = -\|\mathbf{C}_f\tilde{\mathbf{m}}_f\|^2 \leq 0$, $-\tilde{\mathbf{m}}_f^\top\mathbf{D}_f^\top\mathbf{D}_f\tilde{\mathbf{m}}_f = -\|\mathbf{D}_f\tilde{\mathbf{m}}_f\|^2$, and $\|\tilde{\mathbf{m}}_f^\top\mathbf{D}_f^\top\| = \|\mathbf{D}_f\tilde{\mathbf{m}}_f\|$, (61), and Young's inequality, we obtain

$$\begin{aligned}\dot{V}_{\mathbf{m}_f} \leq & -\frac{\eta_{\mathbf{m}}}{2}V_{\mathbf{m}_f}(\tilde{\mathbf{m}}_f, \mathbf{Q}_f) + \eta_{\mathbf{m}}\sigma_r\alpha_{\boldsymbol{\omega}}^2\left\|\frac{dF_{\mathbf{w}}}{d\mathbf{u}}(\hat{\mathbf{u}})\right\|^2 \\ & + \frac{4\alpha_{\boldsymbol{\omega}}^4}{\eta_{\mathbf{m}}}\|\mathbf{Q}_f^{-1}\|\|\mathbf{B}_f\|^2\|\hat{\mathbf{s}} - \mathbf{s}\|^2 + \frac{\eta_{\mathbf{m}}}{4}\|\mathbf{C}_{\Sigma_f}\tilde{\mathbf{m}}_{\mathbf{z}}\|^2 \\ & + \frac{4\alpha_{\mathbf{z}}^2\alpha_{\boldsymbol{\omega}}^4}{\eta_{\mathbf{m}}}\|\mathbf{Q}_f^{-1}\|\|\mathbf{E}_f\|^2|\hat{\upsilon} - \upsilon|^2. \end{aligned} \tag{64}$$

From (24) and (26), the bound $\|\hat{\mathbf{H}}(t, \hat{\mathbf{u}}(t))\| \leq L_{\mathbf{H}}$, and the definition of $\boldsymbol{\omega}$ in (16), which implies that there exists a constant $L_{\boldsymbol{\omega}2} \in \mathbb{R}_{>0}$ such that $\|\boldsymbol{\omega}\| \leq L_{\boldsymbol{\omega}2}$, we obtain

$$\|\hat{\mathbf{s}} - \mathbf{s}\| \leq \frac{1}{\alpha_{\boldsymbol{\omega}}}(L_{\mathbf{H}} + L_{F2})\|\dot{\hat{\mathbf{u}}}\|, |\hat{\upsilon} - \upsilon| \leq \frac{1}{2}(L_{\mathbf{H}} + L_{F2})L_{\boldsymbol{\omega}2}^2. \tag{65}$$

From Assumption 3, we obtain

$$\left\|\frac{dF_{\mathbf{w}}}{d\mathbf{u}}(\hat{\mathbf{u}})\right\| \leq \int_0^1 \left\|\frac{d^2F_{\mathbf{w}}}{d\mathbf{u}d\mathbf{u}^\top}(\sigma\tilde{\mathbf{u}} + \mathbf{u}_{\mathbf{w}}^*)\right\| d\sigma\|\tilde{\mathbf{u}}\| = L_{F2}\|\tilde{\mathbf{u}}\|. \tag{66}$$

Moreover, from the filter design in (28), there exist $L_{\mathbf{B}_{\Sigma_f}}, L_{\mathbf{C}_{\Sigma_f}} \in \mathbb{R}_{>0}$ such that $\|\mathbf{B}_{\Sigma_f}\| \leq L_{\mathbf{B}_{\Sigma_f}}$ and $\|\mathbf{C}_{\Sigma_f}\| \leq L_{\mathbf{C}_{\Sigma_f}}$, respectively. Then, from (34), it follows that $\|\mathbf{E}_f\| = \|\mathbf{B}_{\Sigma_f}\| = L_{\mathbf{B}_{\Sigma_f}}$ and $\|\mathbf{B}_f\| = 1$. Substitution of all these inequalities in (64) yields the following inequality:

$$\begin{aligned}\dot{V}_{\mathbf{m}_f} \leq & -\frac{\eta_{\mathbf{m}}}{2}V_{\mathbf{m}_f}(\tilde{\mathbf{m}}_f, \mathbf{Q}_f) + \eta_{\mathbf{m}}\sigma_r\alpha_{\boldsymbol{\omega}}^2L_{F2}^2\|\tilde{\mathbf{u}}\|^2 \\ & + \frac{4\alpha_{\boldsymbol{\omega}}^2}{\eta_{\mathbf{m}}}(L_{\mathbf{H}} + L_{F2})^2\|\mathbf{Q}_f^{-1}\|\|\dot{\hat{\mathbf{u}}}\|^2 + \frac{\eta_{\mathbf{m}}}{4}L_{\mathbf{C}_{\Sigma_f}}^2\|\tilde{\mathbf{m}}_{\mathbf{z}}\|^2 \\ & + \frac{\alpha_{\mathbf{z}}^2\alpha_{\boldsymbol{\omega}}^4}{\eta_{\mathbf{m}}}L_{\mathbf{B}_{\Sigma_f}}^2(L_{\mathbf{H}} + L_{F2})^2\ L_{\boldsymbol{\omega}2}^4\|\mathbf{Q}_f^{-1}\|. \end{aligned} \tag{67}$$

Let us define $\tilde{y} := y - \bar{y}_{\mathbf{w}}(t, \mathbf{u})$. From Property 1, we can derive the general solution for (31) as follows:

$$\begin{aligned}\tilde{\mathbf{m}}_{\mathbf{z}}(t) = & e^{\alpha_{\mathbf{z}}\mathbf{A}_{\Sigma_f}t}\tilde{\mathbf{m}}_{\mathbf{z}}(0) + \alpha_{\mathbf{z}}\int_0^t e^{\alpha_{\mathbf{z}}\mathbf{A}_{\Sigma_f}(t-\tau)}\mathbf{B}_{\Sigma_f}\tilde{y}(\tau)d\tau \\ & + \alpha_{\mathbf{z}}\int_0^t e^{\alpha_{\mathbf{z}}\mathbf{A}_{\Sigma_f}(t-\tau)}\mathbf{B}_{\Sigma_f}\big(\bar{y}_{\mathbf{w}}(\tau, \mathbf{u}(\tau)) - F_{\mathbf{w}}(\mathbf{u}(\tau))\big)d\tau \end{aligned} \tag{68}$$

for all $t \in \mathbb{R}_{\geq 0}$. The filter Σ_f is designed such that $\alpha_{\mathbf{z}}\mathbf{A}_{\Sigma_f}$ is Hurwitz, i.e., there exist $k, \lambda \in \mathbb{R}_{>0}$ such that $\|e^{\alpha_{\mathbf{z}}\mathbf{A}_{\Sigma_f}(t-\tau)}\| \leq ke^{-\alpha_{\mathbf{z}}\lambda(t-\tau)}$ for all $t \geq \tau$. From this fact, we can bound the second term in (68) by $(k/\lambda)\|\mathbf{B}_{\Sigma_f}\|\sup_{s\in[0,t]}|\tilde{y}(s)|$. For a bound on the third term in (68), we exploit Assumption 2. By defining $\tilde{\mathbf{e}} := \mathbf{e} - \bar{\mathbf{e}}_{\mathbf{w}}(t, \mathbf{u})$, using (6), (9), and the bounds in (8), it follows that:

$$\begin{aligned}|\tilde{y}| \leq & L_{Z\mathbf{e}}\|\bar{\mathbf{e}}_{\mathbf{w}}(t, \mathbf{u}) - \bar{\mathbf{e}}_{\mathbf{w}}(t, \mathbf{u}_{\mathbf{w}}^*)\|\|\tilde{\mathbf{e}}\| + L_{Z*}\|\tilde{\mathbf{e}}\| \\ & + \frac{L_{Z\mathbf{e}}}{2}\|\tilde{\mathbf{e}}\|^2 + L_{Z\mathbf{u}}\|\mathbf{u} - \mathbf{u}_{\mathbf{w}}^*\|\|\tilde{\mathbf{e}}\| \end{aligned} \tag{69}$$

with $L_{Z*} = \|(\partial Z/\partial\mathbf{e})(\bar{\mathbf{e}}_{\mathbf{w}}(t, \mathbf{u}_{\mathbf{w}}^*), \mathbf{u}_{\mathbf{w}}^*)\| \in \mathbb{R}_{>0}$. Moreover, from [14, (2) in Assumption 1], we have that

$$\|\tilde{\mathbf{e}}\| = \|\mathbf{g}(\mathbf{x}, \mathbf{u}, \mathbf{w}) - \mathbf{g}(\bar{\mathbf{x}}_{\mathbf{w}}(t, \mathbf{u}), \mathbf{u}, \mathbf{w})\| \leq L_{\mathbf{gx}}\|\tilde{\mathbf{x}}\| \tag{70}$$

and subsequently, from (3) in Assumption 1, we have that

$$\|\bar{\mathbf{e}}_{\mathbf{w}}(t, \mathbf{u}) - \bar{\mathbf{e}}_{\mathbf{w}}(t, \mathbf{u}_{\mathbf{w}}^*)\| \leq (L_{\mathbf{gu}} + L_{\mathbf{gx}}L_{\mathbf{xu}})\|\mathbf{u} - \mathbf{u}_{\mathbf{w}}^*\|. \tag{71}$$

From (15), it follows that $\|\mathbf{u} - \mathbf{u}_{\mathbf{w}}^*\| \leq \|\tilde{\mathbf{u}}\| + \alpha_{\boldsymbol{\omega}}L_{\boldsymbol{\omega}2}$. Using Young's inequality it follows that $\|\mathbf{u} - \mathbf{u}_{\mathbf{w}}^*\|^2 \leq 2\|\tilde{\mathbf{u}}\|^2 + 2\alpha_{\boldsymbol{\omega}}^2\ L_{\boldsymbol{\omega}2}^2$. Combining (68)–(71), we obtain the following bound on $\|\tilde{\mathbf{m}}_{\mathbf{z}}\|$:

$$\begin{aligned}\|\tilde{\mathbf{m}}_{\mathbf{z}}\| \leq \max\big\{ & 2\ e^{\alpha_{\mathbf{z}}\mathbf{A}_{\Sigma_f}t}\|\tilde{\mathbf{m}}_{\mathbf{z}}(0)\|, c_{mz1}\|\tilde{\mathbf{x}}\|^2 \\ & + 4\alpha_{\mathbf{z}}\delta_{\mathbf{z}2}\|\tilde{\mathbf{u}}\|^2 + (\alpha_{\boldsymbol{\omega}}c_{mz2} + c_{mz3})\|\tilde{\mathbf{x}}\| \\ & + c_{mz4}\|\tilde{\mathbf{u}}\|\|\tilde{\mathbf{x}}\| + 2\alpha_{\mathbf{z}}\delta_{\mathbf{z}1} + \alpha_{\mathbf{z}}\alpha_{\boldsymbol{\omega}}^2\ c_{mz5}\delta_{\mathbf{z}2}\big\} \end{aligned} \tag{72}$$

with $c_{mz1}, \ldots, c_{mz5} \in \mathbb{R}_{>0}$ being positive constants. From [14, Lemmas 17 and 19] we have that, for any finite time $t_1 \geq 0$, the solutions $\tilde{\mathbf{x}}$ and $\tilde{\mathbf{u}}$ are bounded for all $0 \leq t \leq t_1$. Moreover, from Lemma 1, we have that $\mathbf{Q}_f^{-1}$ is positive definite and bounded for all $0 \leq t \leq t_1$. From these facts and $\|\dot{\hat{\mathbf{u}}}\| \leq \eta_{\mathbf{u}}$, which follows from (37), we obtain that the right-hand side of (67) is bounded for all $0 \leq t \leq t_1$. Therefore, since $V_{\mathbf{m}_f}(\tilde{\mathbf{m}}_f, \mathbf{Q}_f)$ will be bounded for all $0 \leq t \leq t_1$ and $\mathbf{Q}_f^{-1}$ is positive definite and bounded for all $0 \leq t \leq t_1$ as well, it follows from (62) that the solutions $\tilde{\mathbf{m}}_f$ are bounded for all $0 \leq t \leq t_1$. Let us define $t_1 \geq 0$ such that, from [14, Lemma 17], Lemma 1, and (72), we have that $\|\tilde{\mathbf{x}}(t)\| \leq \alpha_{\boldsymbol{\omega}}\eta_{\boldsymbol{\omega}}c_{\mathbf{x}2}$ and $\|\tilde{\mathbf{Q}}_f\| \leq (1/8)$, for all $t \geq t_1$. Also, $2\ e^{\alpha_{\mathbf{z}}A_{\Sigma_f}t_1}\|\tilde{\mathbf{m}}_{\mathbf{z}}(0)\|$ in (72) is sufficiently decayed for all $t \geq t_1$. In addition, from (39) and sufficiently small ϵ_5, we have that $(1/4)\mathbf{I} \preceq \mathbf{Q}_f^{-1} \preceq (5/4)\mathbf{I}$ for all $t \geq t_1$ and all $\sigma_r \leq \epsilon_5$. From (62), it follows that $(1/4)\|\tilde{\mathbf{m}}_f\|^2 \leq V_{\mathbf{m}_f}(\tilde{\mathbf{m}}_f, \mathbf{Q}_f) \leq (5/4)\|\tilde{\mathbf{m}}_f\|^2$, for all $t \geq t_1$, and $\|\mathbf{Q}_f^{-1}\| \leq (5/4)$ for all $t \geq t_1$. From (27), (32), (39), $\|\mathbf{D}_f\| = 1$, and the bound in (14), it follows that $\|\dot{\hat{\mathbf{u}}}\|^2 \leq 8\lambda_{\mathbf{u}}^2\ V_{\mathbf{m}_f}(\tilde{\mathbf{m}}_f, \mathbf{Q}_f) + 2\alpha_{\boldsymbol{\omega}}^2\lambda_{\mathbf{u}}^2\ L_{F2}^2\|\tilde{\mathbf{u}}\|^2$, for all $t_1 \geq 0$. From this fact, and taking ϵ_3 in Theorem 1 sufficiently small, we obtain

$$\begin{aligned}\dot{V}_{\mathbf{m}_f} \leq & -\frac{\eta_{\mathbf{m}}}{4}V_{\mathbf{m}_f}(\tilde{\mathbf{m}}_f, \mathbf{Q}_f) + \eta_{\mathbf{m}}\sigma_r\alpha_{\boldsymbol{\omega}}^2L_{F2}^2\|\tilde{\mathbf{u}}\|^2 \\ & + 10\eta_{\mathbf{m}}\alpha_{\boldsymbol{\omega}}^2\frac{\alpha_{\boldsymbol{\omega}}^2\lambda_{\mathbf{u}}^2}{\eta_{\mathbf{m}}^2}L_{F2}^2(L_{\mathbf{H}} + L_{F2})^2\|\tilde{\mathbf{u}}\|^2 \\ & + \frac{6}{4}\eta_{\mathbf{m}}\alpha_{\boldsymbol{\omega}}^4\eta_{\boldsymbol{\omega}}^4\ L_{\mathbf{C}_{\Sigma_f}}^2c_{mz1}^2\ c_{\mathbf{x}2}^4 + 24\eta_{\mathbf{m}}\alpha_{\mathbf{z}}^2\ L_{\mathbf{C}_{\Sigma_f}}^2\delta_{\mathbf{z}2}^2\|\tilde{\mathbf{u}}\|^4 \\ & + \frac{6}{4}\eta_{\mathbf{m}}\alpha_{\boldsymbol{\omega}}^2\eta_{\boldsymbol{\omega}}^2\ L_{\mathbf{C}_{\Sigma_f}}^2(\epsilon_0\ c_{mz2} + c_{mz3})^2\ c_{\mathbf{x}2}^2 \\ & + \frac{6}{4}\eta_{\mathbf{m}}\alpha_{\boldsymbol{\omega}}^2\eta_{\boldsymbol{\omega}}^2\ L_{\mathbf{C}_{\Sigma_f}}^2\ c_{mz4}^2\ c_{\mathbf{x}2}^2\|\tilde{\mathbf{u}}\|^2 \\ & + \frac{6}{4}\eta_{\mathbf{m}}\alpha_{\mathbf{z}}^2\alpha_{\boldsymbol{\omega}}^4\ L_{\mathbf{C}_{\Sigma_f}}^2\ c_{mz5}^2\delta_{\mathbf{z}2}^2 \\ & + 6\eta_{\mathbf{m}}\alpha_{\mathbf{z}}^2\ L_{\mathbf{C}_{\Sigma_f}}^2\delta_{\mathbf{z}1}^2 + \frac{5}{4}\eta_{\mathbf{m}}\frac{\alpha_{\mathbf{z}}^2\alpha_{\boldsymbol{\omega}}^4}{\eta_{\mathbf{m}}^2}L_{\mathbf{B}_{\Sigma_f}}^2(L_{\mathbf{H}} + L_{F2})^2L_{\boldsymbol{\omega}2}^4 \end{aligned} \tag{73}$$

for all $t \geq t_1$, $\alpha_{\mathbf{z}} \leq \eta_{\mathbf{m}}\epsilon_2$, and all $\alpha_\omega\lambda_{\mathbf{u}} \leq \eta_{\mathbf{m}}\epsilon_3$. From the comparison lemma and (62), we obtain

$$\begin{aligned}
&\sup_{t\geq t_1}\|\tilde{\mathbf{m}}_f(t)\| \leq 2\sqrt{10}\sup_{t\geq t_1}\max\Bigg\{\sqrt{\frac{5}{4}}\|\tilde{\mathbf{m}}_f(t_1)\| \\
&2\sqrt{\sigma_r}\alpha_\omega L_{F2}\|\tilde{\mathbf{u}}(t)\|, \sqrt{40}\alpha_\omega\frac{\alpha_\omega\lambda_{\mathbf{u}}}{\eta_{\mathbf{m}}}L_{F2}(L_{\mathbf{H}}+L_{F2})\|\tilde{\mathbf{u}}(t)\| \\
&4\sqrt{6}\alpha_{\mathbf{z}}L_{\mathbf{C}_{\Sigma_f}}\delta_{\mathbf{z}2}\|\tilde{\mathbf{u}}(t)\|^2, \sqrt{6}\alpha_\omega\eta_\omega L_{\mathbf{C}_{\Sigma_f}}c_{mz4}c_{\mathbf{x}2}\|\tilde{\mathbf{u}}(t)\| \\
&\sqrt{6}\alpha_\omega^2\eta_\omega^2\ L_{\mathbf{C}_{\Sigma_f}}c_{mz1}c_{\mathbf{x}2}^2, \sqrt{6}\alpha_{\mathbf{z}}\alpha_\omega^2\ L_{\mathbf{C}_{\Sigma_f}}c_{mz5}\delta_{\mathbf{z}2} \\
&\sqrt{6}\alpha_\omega\eta_\omega L_{\mathbf{C}_{\Sigma_f}}(\epsilon_0\ c_{mz2}+c_{mz3})c_{\mathbf{x}2}, 2\sqrt{6}\alpha_{\mathbf{z}}L_{\mathbf{C}_{\Sigma_f}}\delta_{\mathbf{z}1} \\
&\sqrt{5}\alpha_\omega^2\epsilon_2\ L_{\mathbf{B}_{\Sigma_f}}(L_{\mathbf{H}}+L_{F2})L_{\omega 2}^2\Bigg\} \qquad (74)
\end{aligned}$$

$$\begin{aligned}
&\limsup_{t\to\infty}\|\tilde{\mathbf{m}}_f(t)\| \leq 2\sqrt{10}\limsup_{t\to\infty} \\
&\max\Bigg\{2\sqrt{\sigma_r}\alpha_\omega L_{F2}\|\tilde{\mathbf{u}}(t)\|, \sqrt{40}\alpha_\omega\frac{\alpha_\omega\lambda_{\mathbf{u}}}{\eta_{\mathbf{m}}}L_{F2}(L_{\mathbf{H}}+L_{F2})\|\tilde{\mathbf{u}}(t)\| \\
&4\sqrt{6}\alpha_{\mathbf{z}}L_{\mathbf{C}_{\Sigma_f}}\delta_{\mathbf{z}2}\|\tilde{\mathbf{u}}(t)\|^2, \sqrt{6}\alpha_\omega\eta_\omega L_{\mathbf{C}_{\Sigma_f}}c_{mz4}c_{\mathbf{x}2}\|\tilde{\mathbf{u}}(t)\| \\
&\sqrt{6}\alpha_\omega^2\eta_\omega^2\ L_{\mathbf{C}_{\Sigma_f}}c_{mz1}c_{\mathbf{x}2}^2, \sqrt{6}\alpha_{\mathbf{z}}\alpha_\omega^2\ L_{\mathbf{C}_{\Sigma_f}}c_{mz5}\delta_{\mathbf{z}2} \\
&\sqrt{6}\alpha_\omega\eta_\omega L_{\mathbf{C}_{\Sigma_f}}(\epsilon_0\ c_{mz2}+c_{mz3})c_{\mathbf{x}2}, 2\sqrt{6}\alpha_{\mathbf{z}}L_{\mathbf{C}_{\Sigma_f}}\delta_{\mathbf{z}1} \\
&\sqrt{5}\alpha_\omega^2\epsilon_2\ L_{\mathbf{B}_{\Sigma_f}}(L_{\mathbf{H}}+L_{F2})L_{\omega 2}^2\Bigg\} \qquad (75)
\end{aligned}$$

for all $t \geq t_1$, all $\alpha_\omega \leq \epsilon_0$, all $\eta_\omega \leq \alpha_{\mathbf{z}}\epsilon_1$, all $\alpha_{\mathbf{z}} \leq \eta_{\mathbf{m}}\epsilon_2$, all $\alpha_\omega\lambda_{\mathbf{u}} \leq \eta_{\mathbf{m}}\epsilon_3$, all $\eta_{\mathbf{u}} \leq \alpha_\omega\eta_\omega\epsilon_4$, and all $\sigma_r \leq \epsilon_5$. This completes the proof of Lemma 2. □

REFERENCES

[1] R. Antonello, R. Oboe, L. Prandi, and F. Biganzoli, "Automatic mode matching in MEMS vibrating gyroscopes using extremum-seeking control," *IEEE Trans. Ind. Electron.*, vol. 56, no. 10, pp. 3880–3891, Oct. 2009.

[2] K. B. Ariyur and M. Krstić, *Real Time Optimization by Extremum Seeking Control*. New York, NY, USA: Wiley, 2003.

[3] A. S. Bazanella, L. Campestrini, and D. Eckhard, *Data-Driven Controller Design: The H_2 Approach*. New York, NY, USA: Springer, 2012.

[4] H. Butler, "Position control in lithographic equipment: An enabler for current-day chip manufacturing," *IEEE Syst. Control*, vol. 31, no. 5, pp. 28–47, May 2011.

[5] M. C. Campi, A. Lecchini, and S. M. Savaresi, "Virtual reference feedback tuning: A direct method for the design of feedback controllers," *Automatica*, vol. 38, no. 8, pp. 1337–1346, Aug. 2002.

[6] Z. Cao, H. B. Dürr, C. Ebenbauer, F. Allgöwer, and F. Gao, "Iterative learning and extremum seeking for repetitive time-varying mappings," *IEEE Trans. Autom. Control*, vol. 62, no. 7, pp. 3339–3353, Jul. 2017.

[7] J. Freudenberg, R. Middleton, and A. Stefanpoulou, "A survey of inherent design limitations," in *Proc. Amer. Control Conf.*, vol. 5, Jun. 2000, pp. 2987–3001.

[8] L. Fu and Ü. Özgüner, "Extremum seeking with sliding mode gradient estimation and asymptotic regulation for a class of nonlinear systems," *Automatica*, vol. 47, no. 12, pp. 2595–2603, Dec. 2011.

[9] V. Grushkovskaya, H.-B. Dürr, C. Ebenbauer, and A. Zuyev, "Extremum seeking for time-varying functions using Lie bracket approximations," *IFAC-PapersOnLine*, vol. 50, no. 1, pp. 5522–5528, 2017.

[10] M. Guay, D. Dochain, M. Perrier, and N. Hudon, "Flatness-based extremum-seeking control over periodic orbits," *IEEE Trans. Autom. Control*, vol. 52, no. 10, pp. 2005–2012, Oct. 2007.

[11] M. A. M. Haring, "Extremum-seeking control: Convergence improvements and asymptotic stability," Ph.D. dissertation, Dept. Eng. Cybern., Norwegian Univ. Sci. Technology, Trondheim, Norway, 2016.

[12] M. Haring, N. van de Wouw, and D. Nešić, "Extremum-seeking control for nonlinear systems with periodic steady-state outputs," *Automatica*, vol. 49, no. 6, pp. 1883–1891, Jun. 2013.

[13] L. Hazeleger, M. Haring, and N. van de Wouw, "Extremum-seeking control for steady-state performance optimization of nonlinear plants with time-varying steady-state outputs," in *Proc. Annu. Amer. Control Conf. (ACC)*, Jun. 2018, pp. 2990–2995.

[14] L. Hazeleger, M. Haring, and N. van de Wouw, "Extremum-seeking control for optimization of time-varying steady-state responses of nonlinear systems," *Automatica*, vol. 119, Sep. 2020, Art. no. 109068.

[15] M. Heertjes, T. Tepe, and H. Nijmeijer, "Multi-variable iterative tuning of a variable gain controller with application to a scanning stage system," in *Proc. Amer. Control Conf.*, Jun. 2011, pp. 816–820.

[16] M. F. Heertjes, X. G. P. Schuurbiers, and H. Nijmeijer, "Performance-improved design of N-PID controlled motion systems with applications to wafer stages," *IEEE Trans. Ind. Electron.*, vol. 56, no. 5, pp. 1347–1355, May 2009.

[17] J. P. Hespanha and A. S. Morse, "Switching between stabilizing controllers," *Automatica*, vol. 38, no. 11, pp. 1905–1917, Nov. 2002.

[18] H. Hjalmarsson, M. Gevers, S. Gunnarsson, and O. Lequin, "Iterative feedback tuning: Theory and applications," *IEEE Control Syst.*, vol. 18, no. 4, pp. 26–41, Aug. 1998.

[19] H. Hjalmarsson, S. Gunnarsson, and M. Gevers, "A convergent iterative restricted complexity control design scheme," in *Proc. 33rd IEEE Conf. Decis. Control*, vol. 2, Dec. 1994, pp. 1735–1740.

[20] B. Hunnekens, A. D. Dino, N. van de Wouw, N. van Dijk, and H. Nijmeijer, "Extremum-seeking control for the adaptive design of variable gain controllers," *IEEE Trans. Control Syst. Technol.*, vol. 23, no. 3, pp. 1041–1051, May 2015.

[21] B. G. B. Hunnekens, M. F. Heertjes, N. van de Wouw, and H. Nijmeijer, "Performance optimization of piecewise affine variable-gain controllers for linear motion systems," *Mechatronics*, vol. 24, no. 6, pp. 648–660, Sep. 2014.

[22] A. Karimi, L. Miskovic, and D. Bonvin, "Iterative correlation-based controller tuning," *Int. J. Adapt. Control Signal Process.*, vol. 18, no. 8, pp. 645–664, Oct. 2004.

[23] M. Krstić and H.-H. Wang, "Stability of extremum seeking feedback for general nonlinear dynamic systems," *Automatica*, vol. 36, no. 4, pp. 595–601, Apr. 2000.

[24] M. F. Heertjes, N. I. Perdiguero, and D. A. Deenen, "Robust control and data-driven tuning of a hybrid integrator-gain system with applications to wafer scanners," *Int. J. Adapt. Control Signal Process.*, vol. 33, no. 2, pp. 371–387, Feb. 2019.

[25] D. Nesic, Y. Tan, W. H. Moase, and C. Manzie, "A unifying approach to extremum seeking: Adaptive schemes based on estimation of derivatives," in *Proc. 49th IEEE Conf. Decis. Control (CDC)*, Dec. 2010, pp. 4625–4630.

[26] A. Pavlov, B. G. B. Hunnekens, N. V. D. Wouw, and H. Nijmeijer, "Steady-state performance optimization for nonlinear control systems of Luré type," *Automatica*, vol. 49, no. 7, pp. 2087–2097, Jul. 2013.

[27] A. V. Pavlov, N. van de Wouw, and H. Nijmeijer, *Uniform Output Regulation of Nonlinear Systems: A Convergent Dynamics Approach*. Boston, MA, USA: Birkhäuser, 2006.

[28] F. D. Sahneh, G. Hu, and L. Xie, "Extremum seeking control for systems with time-varying extremum," in *Proc. 31st Chin. Control Conf.*, Jul. 2012, pp. 225–231.

[29] A. Scheinker, "Application of extremum seeking for time-varying systems to resonance control of RF cavities," *IEEE Trans. Control Syst. Technol.*, vol. 25, no. 4, pp. 1521–1528, Jul. 2017.

[30] A. Scheinker, X. Huang, and J. Wu, "Minimization of betatron oscillations of electron beam injected into a time-varying lattice via extremum seeking," *IEEE Trans. Control Syst. Technol.*, vol. 26, no. 1, pp. 336–343, Jan. 2018.

[31] A. Scheinker and M. Krstic, "Minimum-seeking for CLFs: Universal semiglobally stabilizing feedback under unknown control directions," *IEEE Trans. Autom. Control*, vol. 58, no. 5, pp. 1107–1122, May 2013.

[32] A. Scheinker and D. Scheinker, "Bounded extremum seeking with discontinuous dithers," *Automatica*, vol. 69, pp. 250–257, Jul. 2016.

[33] A. Scheinker and M. Krstić, "Extremum seeking with bounded update rates," *Syst. Control Lett.*, vol. 63, pp. 25–31, Jan. 2014.

[34] M. M. Seron, J. H. Braslavsky, and G. C. Goodwin, *Fundamental Limitations in Filtering and Control*. London, U.K.: Springer-Verlag, 1997.

[35] M. S. Stanković and D. M. Stipanović, "Extremum seeking under stochastic noise and applications to mobile sensors," *Automatica*, vol. 46, no. 8, pp. 1243–1251, Aug. 2010.

[36] Y. X. Su, D. Sun, and B. Y. Duan, "Design of an enhanced nonlinear PID controller," *Mechatronics*, vol. 15, no. 8, pp. 1005–1024, Oct. 2005.

[37] Y. Tan, W. H. Moase, C. Manzie, D. Nešić, and I. M. Y. Mareels, "Extremum seeking from 1922 to 2010," in *Proc. 29th Chin. Control Conf.*, Jul. 2010, pp. 14–26.

[38] Y. Tan, D. Nešić, and I. Mareels, "On non-local stability properties of extremum seeking control," *Automatica*, vol. 42, no. 6, pp. 889–903, Jun. 2006.

[39] A. R. Teel and D. Popovic, "Solving smooth and nonsmooth multivariable extremum seeking problems by the methods of nonlinear programming," in *Proc. Amer. Control Conf.*, vol. 3, Dec. 2001, pp. 2394–2399.
[40] N. van de Wouw, H. A. Pastink, M. F. Heertjes, A. V. Pavlov, and H. Nijmeijer, "Performance of convergence-based variable-gain control of optical storage drives," *Automatica*, vol. 44, no. 1, pp. 15–27, Jan. 2008.
[41] H.-H. Wang and M. Krstic, "Extremum seeking for limit cycle minimization," *IEEE Trans. Autom. Control*, vol. 45, no. 12, pp. 2432–2436, Dec. 2000.
[42] C. Zhang and R. Ordóñez, "Robust and adaptive design of numerical optimization-based extremum seeking control," *Automatica*, vol. 45, no. 3, pp. 634–646, Mar. 2009.
[43] J. Zheng, G. Guo, and Y. Wang, "Nonlinear PID control of linear plants for improved disturbance rejection," *IFAC Proc. Volumes*, vol. 38, no. 1, pp. 281–286, 2005.

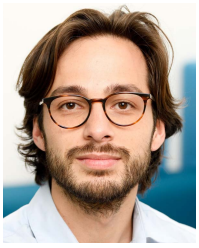

Leroy Hazeleger received the B.Sc. degree in mechanical engineering from the Eindhoven University of Technology, Eindhoven, The Netherlands, in 2012, and the M.Sc. degree in systems and control from the Department of Mechanical Engineering, Eindhoven University of Technology, in 2015. He is currently pursuing the Ph.D. degree with the Dynamics and Control Group, Eindhoven University of Technology.

His current research interests include nonlinear control systems, data-driven optimization, and extremum-seeking control, with applications to high-performance mechatronic systems.

Jeroen van de Wijdeven received the M.Sc. and Ph.D. degrees in mechanical engineering from the Eindhoven University of Technology, Eindhoven, The Netherlands, in 2004 and 2008, respectively.

Since 2008, he has been a Mechatronics Design Engineer at ASML Research, Veldhoven, The Netherlands. His research interests include motion control and dynamics for high-precision mechatronic systems.

Mark Haring received the B.Sc. and M.Sc. degrees in mechanical engineering from the Eindhoven University of Technology, Eindhoven, The Netherlands, in 2008 and 2011, respectively, and the Ph.D. degree in engineering cybernetics from the Norwegian University of Science and Technology (NTNU), Trondheim, Norway, in 2016.

He is currently working as a Research Scientist at SINTEF Digital, Mathematics and Cybernetics, Trondheim. His research interests include automatic control, adaptive control, and estimation.

Nathan van de Wouw (Fellow, IEEE) was born in 1970. He received the M.Sc. (Hons.) and Ph.D. degrees in mechanical engineering from the Eindhoven University of Technology, Eindhoven, The Netherlands, in 1994 and 1999, respectively.

He currently holds a full professor position at the Mechanical Engineering Department, Eindhoven University of Technology. He also holds an adjunct full professor position at the University of Minnesota, Minneapolis, MN, USA. In 2000, he worked at Philips Applied Technologies, Eindhoven. In 2001, he has been working at the Netherlands Organisation for Applied Scientific Research (TNO), Delft, The Netherlands. He has held positions as a Visiting Professor at the University of California Santa Barbara, Santa Barbara, CA, USA, from 2006 to 2007, The University of Melbourne, Melbourne, VIC, Australia, from 2009 to 2010, and the University of Minnesota from 2012 to 2013. He has held a (part-time) full professor position at the Delft University of Technology, Delft, from 2015 to 2019. He has published the books *Uniform Output Regulation of Nonlinear Systems: A convergent Dynamics Approach* with A. V. Pavlov and H. Nijmeijer (Birkhauser, 2005) and *Stability and Convergence of Mechanical Systems with Unilateral Constraints* with R. I. Leine (Springer-Verlag, 2008). His current research interests are the modeling, model reduction, and analysis and control of nonlinear/hybrid and delay systems, with applications to vehicular platooning, high-tech systems, resource exploration, smart energy systems, and networked control systems.

Dr. van de Wouw is an Associate Editor for the journals *Automatica* and IEEE TRANSACTIONS ON CONTROL SYSTEMS TECHNOLOGY. In 2015, he received the IEEE Control Systems Technology Award for the development and application of variable-gain control techniques for high-performance motion systems.